DIPLOMARBEIT

Order equilibrium structures for dipolar fluids

Ausgeführt am Institut für
Theoretische Physik
der Technischen Universität Wien
unter der Anleitung von
Ao. Univ. Prof. Dipl.-Ing. Dr. Gerhard Kahl

durch
Camille Jouvie
39 rue du Flamant Rose
91470 Limours, Frankreich

4. März 2010

Zusammenfassung

Wir haben die Kristallstrukturen des Stockmayer Systems untersucht: hier wechselwirken sphärische, dipolare Teilchen über ein zusätzliches Lennard-Jones Potential. Die geordneten Gleichgewichtstrukturen wurden durch Minimieren des entsprechenden thermodynamischen Potentials, in unserem Fall der freien Enthalpie, ermittelt. Für diese Optimierungsaufgabe haben wir eine sehr verläßliche und effiziente numerische Methode verwendet, die auf Ideen genetischer Algorithmen basiert; letztendlich werden hier Konzepte von Darwins Evolutionstheorie umgesetzt. Für die Berechnung der thermodynamischen Eigenschaften haben wir Ewald Summen verwendet, die insbesondere bei den langreichweitigen Dipol-Wechselwirkungen verläßliche Ergebnisse liefern. Aus rechentechnischen Gründen haben wir uns auf $T = 0$ und räumlich fixierte Dipolmomente eingeschränkt. Mit steigendem Dipolmoment konnten wir insgesamt drei Kristallstrukturen identifizieren: das hexagonale, das raumzentrierte orthorhomibische und das raumzentrierte tetragonale Gitter.

Abstract

We have investigated the crystal structures of the Stockmayer system, where spherical particles, that interact via a Lennard-Jones potential, carry an additional dipole moment. Considering the system at $T = 0$, the ordered equilibrium structures were identified by minimizing the Gibbs free energy with a very efficient and highly reliable optimization algorithm. This numerical tool is based on concepts of evolutionary algorithms, i.e., an approach that uses ideas of Darwin's theory of evolution. For the evaluation of the Gibbs free energy we have used the Ewald summation technique, which enabled us to compute the lattice sum for the long-ranged dipole-dipole interactions in a very efficient way. Keeping for the moment the orientation of the dipoles fixed, we could identify three crystal structures: with increasing dipole moment, we found the hexagonal, the body-centered orthorhombic, and the body-centered tetragonal structures.

Contents

1. Introduction

Dipolar fluids, composed of particles that carry a dipole moment, have provoked a great interest in the soft matter research because of their importance in many domains like technology and biomedicine [1]. A very simple model potential for such a system is the Stockmayer potential, which is the sum of a Lennard-Jones interaction and a dipole-dipole interaction. Due to their relevance in many fields, a complete knowledge of the phase diagram of this system is highly desirable.

The aim of this Master thesis is to provide a contribtion to this phase diagram. To be more specific we focus on the ordered equilibrium structures and restrict ourselves to $T = 0$. This restriction is certainly imposed by numerical limitations. On the other hand we believe that the ground state results will still be valid for low temperature and will then provide a starting point for the full phase diagram of the ordered phases [2]. B. Groh and S. Dietrich [2] have already presented a phase diagram of the ground state completely different from previous studies which only considered the fcc and bct structures [3, 4, 5, 6]. G. T. Gao and X. C. Zeng found that the stable solid phase for the Stockmayer potential near the triple point is the bco structure [7].

Basic laws of thermodynamics impose that the existing structures are those which minimize the thermodynamical potential; in our case it is the Gibbs free energy $G = U + PV - TS$ with

- U the internal energy of the system;
- V its volume;
- S its entropy.

Since the temperature T is considered to be equal to zero, G is reduced to $G = U + PV$.

The minimization of G is non trivial for the two following reasons.

1. The Gibbs free energy of the structures has to be calculated with a high relative

accuracy. On one side, the relative energy differences between two competing structures, fcc and hcp for example, can be of the order of $10^{-5} - 10^{-6}$. On the other side, another difficulty lies in the fact that the dipolar interaction is long-ranged, therefore we can not only take into account the interaction of one particle with its near neighbours. We have to sum over all the particles in the crystal; this infinite sum is not simple to calculate.

2. The search of the crystal structure whith the lowest energy takes place in a high dimensional search space. The description of a crystal via its basis cell requires indeed $6 + 5N$ parameters with N the number of particles in the basis cell: 6 parameters to describe the lattice vectors of the simple unit cell, 3 for the position of each particle and 2 for the orientation of the dipole of each particle. Furthermore, the representation of a crystal by its basis cell is not unique, that is to say, different basis cell can represent the same crystal. Moreover, the energy surface in the search space is rugged, i.e. the energy may change drastically with a little change of one of the parameters.

To cope with the first difficulty, we implemented the Ewald summation [8, 9, 10], which enables to calculate the energy of a system governed by long-ranged interactions. This technique consists in separating the slow-converging sum in real space in two more rapidly converging sums, one in real space, the other one in reciprocal space.

To tackle the second problem, we chose optimization tools based on ideas of evolutionary algorithms as minimization method. These algorithms [11] are a global optimization method which performs an unbiased search in the whole parameter space. In our case, lattices are considered as individuals which are exposed to an artificial evolution. The basic features of the algorithms are based on the ideas of Darwin's theory of evolution : the fittest individuals survive, passing their characteristic features to the next generations, which should be even better adapted. In our case, the "fittest" individuals are those with the lowest Gibbs free energy.

We studied a system of dipolar particles with an absolute dipole value varying from 0 to 12 in reduced units, the dipole of all particles being parallel, under a pressure varying from 0 to $500\epsilon/\sigma^3$ with ϵ and σ the parameters of the Lennard-Jones potential. For a reduced moment value smaller than 3, which is the domain usually studied, we found as in [2] that the system crystallizes either in an hexagonal structure or in a bco structure, and not fcc or bct as assumed in various studies before. For higher dipole values, the system can crystallize in the bct structure.

This thesis is organized in the following way:

- **Chapter 2** presents the model of the Stockmayer potential.
- **Chapter 3** explains the principle of the Ewald summation and its practical implementation in our problem.
- **Chapter 4** presents basic ideas of the evolutionary algorithms and the structure of the algorithm we used in this thesis.
- **Chapter 5** presents the implementation of the Ewald summation in our FORTRAN 90 evolutionary algorithm and the results we obtained.
- **Chapter 6** consists of a short overview of the work we did and points out possible future improvements for our algorithm.

2. Model

The aim of this work is to determine with the help of optimization techniques based on genetic algorithms the crystal structure of spherical dipolar particles considered interacting via the Stockmayer potential. Such an interaction is, for example, encountered for particles in electro- or magneto-rheological fluids, or ferrofluids like the magnetite Fe_3O_4. Those systems are considered to have a high potential for technology and biomedicine [1].

The quantity which has to be minimized in order to obtain the ordered stucture of minimum energy is the Gibbs free energy G:

$$G = U + PV - TS \tag{2.1}$$

with

- U the internal energy of the system;
- V its volume;
- S its entropy.

Throughout, the temperature T is considered to be equal to zero, so G is reduced to $G = U + PV$.

2.1. Stockmayer potential

The Stockmayer potential is the sum of the Lennard-Jones potential and of the dipolar interaction potential. In the Stockmayer (12-6-3) model, which is used here, the interaction energy of a pair of particles is given by

$$V_{pair}(r) = 4\epsilon\Big[\Big(\frac{\sigma}{r}\Big)^{12} - \Big(\frac{\sigma}{r}\Big)^{6} - \delta\Big(\frac{\sigma}{r}\Big)^{3}\Big] \tag{2.2}$$

where:

- $r = |r_1 - r_2|$, the distance between the centres of mass of the two particles;
- ϵ is the minimum in the Lennard-Jones potential (ϵ has the dimension of an energy);
- σ is the diameter of the particles (length), i.e. the value of r at which $V_{pair}(r)$ vanishes;
- δ (energy) depends on the strength of the dipoles and on their orientation.

Additional factors, such as $4\pi\epsilon_0$, are omitted for simplicity of notation. An alternative to the Stockmayer potential is to use a soft sphere or a hard sphere [12] potential instead of the Lennard-Jones potential.

2.2. Lennard-Jones potential

The Lennard-Jones (12-6) potential (see fig.2.1) is given by

$$V_{\mathrm{LJ,pair}}(r) = 4\epsilon\Big[\Big(\frac{\sigma}{r}\Big)^{12} - \Big(\frac{\sigma}{r}\Big)^{6}\Big] \tag{2.3}$$

$$= V^{(12)}_{SS,pair}(r) - V^{(6)}_{SS,pair}(r) \tag{2.4}$$

where $V^{(n)}_{SS,pair} = 4\epsilon\Big(\frac{\sigma}{r}\Big)^{n}$ represents the purely repulsive soft sphere (SS) potential. The Lennard-Jones potential represents a reasonable model that describes the interaction between a pair of neutral atoms or molecules. It was proposed in 1924 by John Lennard-Jones [13] and is commonly used to describe the interactions between rare gas particles.

In $V_{\mathrm{LJ,pair}}(r)$, the term $4\epsilon\Big(\frac{\sigma}{r}\Big)^{6}$ describes an attractive potential which becomes relevant at large distances, it can be derived from the van der Waals or dispersion forces.

The term $4\epsilon\Big(\frac{\sigma}{r}\Big)^{12}$ takes into account Pauli repulsion at short ranges due to overlapping electron orbitals. The explicit form of this term has no theoretical explanation; an exponential dependency on the distance would be more suitable, but the exponent 12 was chosen because of computationnal convenience: r^{-12} is the square of r^{-6}.

Others exponents can also be used instead of 6 and 12.

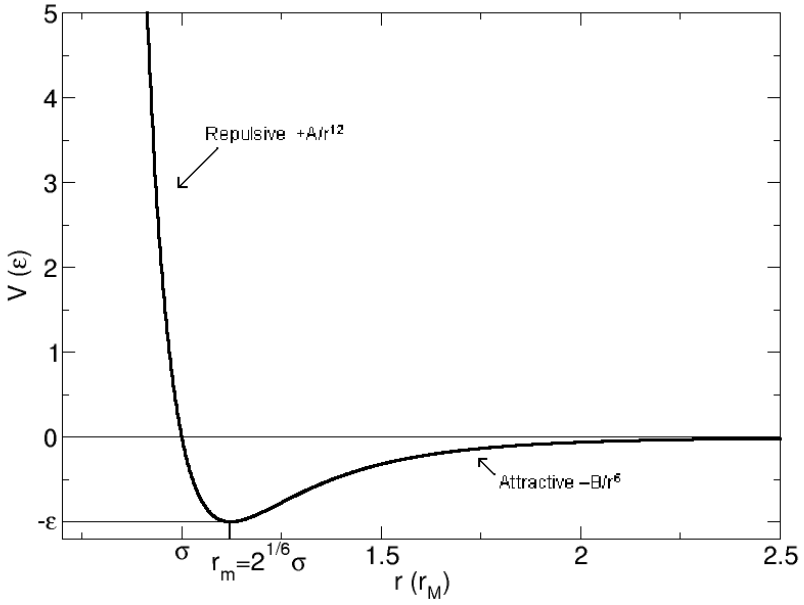

Figure 2.1.: 12-6-Lennard-Jones-Potential

2.3. Dipolar potential

The dipolar contribution to the Stockmayer potential is given by

$$V_{\text{dipolar,pair}}(\mathbf{r}_{ij};\boldsymbol{\mu}_i,\boldsymbol{\mu}_j) = -4\epsilon\delta\Big(\frac{\sigma}{r}\Big)^3 = \frac{\boldsymbol{\mu}_i\cdot\boldsymbol{\mu}_j}{r_{ij}^3} - 3\frac{(\boldsymbol{\mu}_i\cdot\mathbf{r}_{ij})(\boldsymbol{\mu}_j\cdot\mathbf{r}_{ij})}{r_{ij}^5} \tag{2.5}$$

$$= -\frac{\|\mu\|^2}{r^3}(2\cos\theta_1\cos\theta_2 - \sin\theta_1\sin\theta_2\cos\phi) \tag{2.6}$$

where

- θ_1 and θ_2 are the inclinations of the two dipole axes with respect to the intermolecular axis (see fig.2.2);
- ϕ is the azimuth angle between the two dipole moments $\boldsymbol{\mu}_i$.

$V_{\text{dipolar,pair}}(\mathbf{r}_{ij};\boldsymbol{\mu}_i,\boldsymbol{\mu}_j)$ describes the interaction between two particles i and j carrying magnetic moments $\boldsymbol{\mu}_i$ and $\boldsymbol{\mu}_j$. The parameters can be determined experimentally or fitted to reproduce quantum chemistry calculations; they depend on the nature of the particle [14]. Since the dipolar interaction is anisotropic and can be both attractive as well as repulsive, the properties of a dipolar system are not easy to predict. However, it seems that even for strongly confined dipolar fluids, this interaction manifests itself as a net attraction [15]. Having $\mu^* = \sqrt{\frac{\mu^2}{\sigma^3 k_B T}}$ with k_B the Boltzmann constant, one

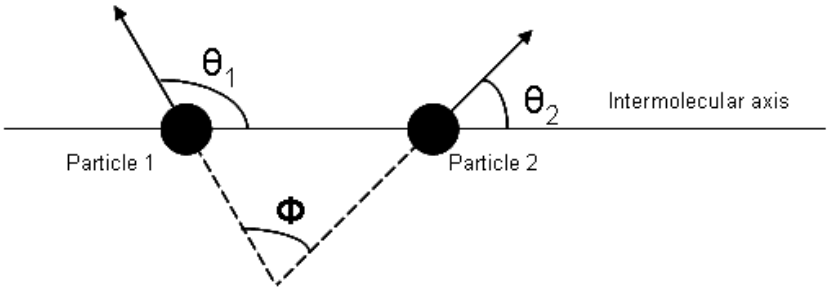

Figure 2.2.: Angles used in the dipolar potential formula

can define the dimensionless coupling parameter $\lambda = \mu^{*2}$, which is half of the ratio of the dipolar energy of two aligned dipoles at close contact to the thermal energy. This parameter permits to dinstinguish between two sorts of behaviour [12]:

- For $\lambda < 1$, the magnetic interaction is weak. This situation corresponds to most of the conventional ferrofluids, like the magnetite, with a particle size of 5-10 nm. Under these conditions and in zero field the dipolar part plays a minor role and the particles behave essentially like non-magnetic ones.
- For $\lambda >> 1$, the dipolar interaction is strong and the formation of clusters and chains is observed. Magnetic colloids with a λ value of up to 70 have been found in bacteria [16].

2.4. Extended expression of the Stockmayer potential

Finally, the total interparticle potential in a Stockmayer system is given by

$$V_{\text{Stockmayer,pair}}(\mathbf{r}_{ij};\boldsymbol{\mu}_i,\boldsymbol{\mu}_j) = 4\epsilon\Big[\Big(\frac{\sigma}{r}\Big)^{12} - \Big(\frac{\sigma}{r}\Big)^{6}\Big] + \frac{\boldsymbol{\mu}_i\cdot\boldsymbol{\mu}_j}{r_{ij}^3} - 3\frac{(\boldsymbol{\mu}_i\cdot\mathbf{r}_{ij})(\boldsymbol{\mu}_j\cdot\mathbf{r}_{ij})}{r_{ij}^5}. \tag{2.7}$$

The ground state properties only depend on the reduced dipole moment $m^* = \sqrt{\mu^2/(\sigma^3\epsilon)}$ and the reduced particle density $\rho^* = \sigma^3 N/V$ of N particles in the volume V. The ground state energy per particle U has then the form $U_{\text{Stockmayer}} = \epsilon\hat{E}(\rho^*, m^*)$ where $\hat{E}$ is a dimensionless scaling functions which contains all the structure dependence.

2.4.1. Energy of a crystal basis cell

If we consider a crystal, the structure is given according to Bravais [17] by the geometry of a basis cell and by the number, the types and the positions of the particles in this basis cell. The geometry of the cell can be given by the length of the sides and the three angles between these sides (see figure 2.3). If the primitive vectors that span the basis cell are called **a**,**b** and **c**, the position of each lattice point in relation to the origin is given by $\mathbf{R} = n_a \cdot \mathbf{a} + n_b \cdot \mathbf{b} + n_c \cdot \mathbf{c}$ with $(n_a, n_b, n_c) \in \mathbb{Z}^3$.

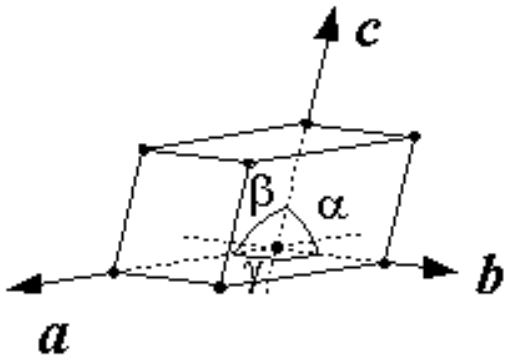

Figure 2.3.: Schematic representation of a Bravais lattice

Periodic boudary conditions are applied on the system. Due to the reduced symmetry compared to the nonpolar case the crystals are never strictly cubic.

The energy of the basis cell is

$$U = U_D + U_{LJ} = \frac{1}{2} \sum_{i=1}^{N} \sum_{j=1}^{N} \sum_{\mathbf{R}}{}' [\mathrm{V}_{\mathrm{dipolar,pair}}(\mathbf{R} + \mathbf{r}_{\mathrm{ij}}; \boldsymbol{\mu}_{\mathrm{i}}, \boldsymbol{\mu}_{\mathrm{j}}) + \mathrm{V}_{\mathrm{LJ,pair}}(\mathbf{R} + \mathbf{r}_{\mathrm{ij}})] \quad (2.8)$$

with

- U the total energy of the basis cell;
- U_D the total dipolar energy of the basis cell;
- U_{LJ} the total Lennard Jones energy of the basis cell;
- $V_{\mathrm{dipolar,pair}}(\mathbf{R} + \mathbf{r}_{ij}; \boldsymbol{\mu}_i, \boldsymbol{\mu}_j)$ the dipolar energy of the interaction between two particles;

- $V_{\mathrm{LJ,pair}}(\mathbf{R} + \mathbf{r}_{ij})$ the Lennard-Jones energy of the interaction between two particles;
- N the number of particles in the basis cell;
- $\mathbf{r}_{ij}$ the vector between two particles i and j in the central basis cell;
- $\mathbf{R}$ a lattice vector. The prime indicates that the $i = j$ term must be omitted for $R = 0$ in order to avoid self-interaction of the particles.

3. Ewald sums

3.1. Stockmayer potential: a long-range interaction

The lattice sum of the dipolar potential given by

$$U_D = \frac{1}{2}\sum_{i=1}^{N}\sum_{j=1}^{N} V_{\text{dipolar,pair}}(\mathbf{r};\boldsymbol{\mu}_i,\boldsymbol{\mu}_j) \tag{3.1}$$

with

$$V_{\text{dipolar,pair}}(\mathbf{r};\boldsymbol{\mu}_i,\boldsymbol{\mu}_j) = \frac{\boldsymbol{\mu}_i\cdot\boldsymbol{\mu}_j}{r^3} - 3\frac{(\boldsymbol{\mu}_i\cdot\mathbf{r})(\boldsymbol{\mu}_j\cdot\mathbf{r})}{r^5}, \tag{3.2}$$

and N the total number of particles of the system is long-ranged, which brings along the following problem: in one hand, the interaction between particles decays as $1/r^3$, but, in the other hand, the number of particles grows with r^3; thus the product of the two does not decrease with r. A straightforward numerical calculation of lattice sums is hampered by their slow convergence. In the other hand a simple truncation of the infinite sum over all particles leads to substantial and unwanted modifications of the physics of the problem since the particles located far from a tagged particle still interact with it. To speed up the convergence of the evaluation of the lattice sum and avoid this direct truncation the Ewald technique [8, 9, 10] is employed.

For the Lennard-Jones contribution to the lattice sum, an acceleration of the convergence is not needed due to rapid decay with distance; however using the Ewald sums is convenient to avoid the cut-off at r=0 which is necessary for the direct sum.

Nevertheless, the direct sum, which is easy to implement, but computationally very expensive, is implemented in order to test the correctness of the Ewald sum method [18].

3.2. Principle of the Ewald summation

The Ewald summation technique [8, 9, 10] applies to any periodic system. Its basic idea is to separate a slow-converging sum into two more rapidly - even exponentially - converging sums. This method is especially applied for long range interactions such as the dipolar or the Coulombic interactions.

In an effort to evaluate $\sum_{\mathbf{r}} f(\mathbf{r})$ accurately, one writes $f(\mathbf{r}) = h(\mathbf{r}) + g(\mathbf{r})$ where h($\mathbf{r}$) decays rapidly in real space while the Fourier transform $\tilde{g}(\mathbf{k}) = \int d^3r \exp(-i\mathbf{k}\cdot\mathbf{r})g(\mathbf{r})$ decays rapidly in reciprocal space [19]. The sum over $g(\mathbf{r})$ is then evaluated in reciprocal space using the Poisson summation formula. Typically, $f(\mathbf{r}) = (f(\mathbf{r}) - g(\mathbf{r})) + g(\mathbf{r})$, where g($\mathbf{r}$) is a Gaussian dipolar (or charge) distribution which is of the opposite sign but of the same absolute value as the point dipole (or charge) f($\mathbf{r}$) (see figure 3.1). The screened interactions, $f(\mathbf{r}) - g(\mathbf{r})$, are now short-ranged.

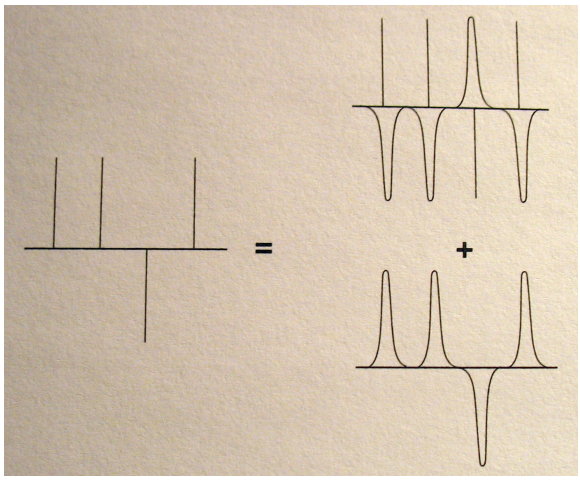

Figure 3.1.: Ewald summation: A slow converging sum of point dipoles in real space (left) is separated into a fast converging sum of screened dipoles in real space (right top panel) and a fast converging sum of Gaussian distributions of dipoles in reciprocal space (right bottom panel) [20]

3.3. Ewald formula

For the sum $\sum_{\mathbf{r}\neq 0} \frac{1}{r^n}$, having $f(\mathbf{r}) = r^{-n}$ and using $h(\mathbf{r}) = \Gamma(n/2, \nu^2 r^2)/[r^n \Gamma(n/2)]$, where $\Gamma(x)$ is the Gamma function and $\Gamma(a, x)$ the incomplete Gamma function, one

obtains [2]

$$\sum_{\mathbf{r}\neq 0}\frac{1}{r^n} = \frac{1}{\Gamma(n/2)}\Bigg[\sum_{\mathbf{r}\neq 0}\frac{1}{r^n}\Gamma(n/2,\nu^2 r^2) + \frac{\pi^{\frac{3}{2}}}{V_c}\sum_{\mathbf{k}\neq 0}\left(\frac{k}{2}\right)^{n-3}\Gamma\left(\frac{3-n}{2},\frac{k^2}{4\nu^2}\right) - \frac{2}{n}\nu^n + N\frac{2}{n-3}\frac{\pi^{\frac{3}{2}}}{V_c}\nu^{n-3}\Bigg] \tag{3.3}$$

with

- $\mathbf{k}$ wavevector;
- V_c volume of the basis cell;
- ν a parameter related to the width of the Gaussian distribution.

The first term in equation (3.3) represents the sum in real space, the second the reciprocal or Fourier space sum. The last two contributions take into account the omissions of the terms $r = 0$ and $k = 0$.

When we consider a crystal with a basis cell of N particles, we obtain for $U^{(n)}_{\text{SS,basis cell}}$, the soft-sphere energy of the basis cell:

$$U^{(n)}_{\text{SS,basis cell}} = \frac{2\epsilon\sigma^n}{\Gamma(n/2)}\sum_{i=1}^{N}\Bigg[\sum_{j=1}^{N}{\sum_{\mathbf{R}}}' \frac{\Gamma(\mathrm{n}/2,\nu^2(\mathbf{R}+\mathbf{r}_{\mathrm{ij}})^2)}{\|\mathbf{R}+\mathbf{r}_{\mathrm{ij}}\|^{\mathrm{n}}} + \frac{\pi^{\frac{3}{2}}}{V_c}\sum_{\mathbf{k}\neq 0}\sum_{j=1}^{N}\cos(\mathbf{k}\cdot\mathbf{r}_{ij})\left(\frac{k}{2}\right)^{n-3}\Gamma\left(\frac{3-n}{2},\frac{k^2}{4\nu^2}\right) - \frac{2}{n}\nu^n + N\frac{2}{n-3}\frac{\pi^{\frac{3}{2}}}{V_c}\nu^{n-3}\Bigg] \tag{3.4}$$

with

- the sum over $\mathbf{R}$ being a sum over the lattice vectors: $\mathbf{R} = n_a\cdot\mathbf{a} + n_b\cdot\mathbf{b} + n_c\cdot\mathbf{c}$ with $(n_a, n_b, n_c) \in \mathbb{Z}^3$. These lattice vectors are generated by the periodic replication of the original cell.
- $\mathbf{r}_{ij}$=$\mathbf{r}_i$-$\mathbf{r}_j$ with i and j particles in the central basis cell.

The Ewald sums of the Lennard-Jones potential and the dipolar potential have similar forms and can be seen in Appendix B.1.

Due to the slow decay of the dipolar potential with distance, the dipolar lattice sum is actually only conditionally convergent in three dimensions, i.e., the value

of the sum is not well defined unless one specifies the order in which the terms are summed up (spheric, cubic...) and the conditions outside the system studied (vacuum, dielectric...) [9, 21].

3.4. Parameters of the Ewald sum

The sums over $\mathbf{R}$ and $\mathbf{k}$ include an infinite number of terms, however in actual calculations we have to keep only a finite number of vectors. Three parameters occur in the Ewald sums that are relevant for this evaluation: the splitting parameter ν, k_{max} and R_{max}. They control the accuracy of the result. We can choose one of these parameters; the two others will then be fixed by the desired precision. The exponential convergence of the sums allows the introduction of relatively small cut offs k_{max} and R_{max} without much loss of accuracy: typically a few hundred or thousand lattice vectors in real and reciprocal space are sufficient to obtain machine precision (10^{-16}) [2].

R_{max} can be a positive integer or a vector $(R_{max,a}, R_{max,b}, R_{max,c})$, if the cut off in R is not the same in all three directions. The maximal value of $\|R\|$ in direction $\mathbf{a}$ will be, in the first case, $R_{max} \cdot \|a\|$, and in the second case $R_{max,a} \cdot \|a\|$.

k_{max} can as well be a positive integer or a vector $(k_{max,a}, k_{max,b}, k_{max,c})$.

ν is a positive real number related to the width of the Gaussian curve g. This parameter tunes the relative weight of the real and reciprocal space contributions. If the value of ν is large, the Gaussian distribution is narrow and so the real space sum converges fast; this mean that a small R_{max} is sufficient for a rapid convergence. On the other hand, a small value of ν causes the reciprocal space sum to converge faster, i.e. a small k_{max} will be sufficent.

If we consider an infinite Ewald sum, ν can be chosen arbitrarily because the results do not depend on this parameter. However, as we compute a finite sum, there is only a small range of values of ν for which the sum really does not depend on this parameter. The optimal value, as for the other parameters, has to be found experimentally. In practice, ν may be chosen such that both sums converge approximately with the same rate, or that the errors accumulated in the two contributions are equal. The error on the contribution of the real space and the one on the contribution of the reciprocal space depend very sensitively on ν.

Usually R_{max} is chosen first. Then ν is chosen so that for this value of ν the real space terms are negligible for $R > R_{max}$. Finally k_{max} is chosen so that for this value of ν the reciprocal space terms are negligible for $k > k_{max}$. As the calculations in the reciprocal space are faster than in the real space, it is common to use the minimum image convention: $R_{max} < L/2$ with L being the width of the simulation box - in our case L would be the lenght of a side of a cubic basis cell. Thus, nearly the whole calculation is carried out in reciprocal space (R_{max}=0) [22]. Because of the accuracy it is then recommended to assure $\nu \geq 3.2/R_{max}$ [23]. This method is used in molecular dynamics (MD) or Monte Carlo (MC) simulations, where the number of particles in the simulation box is at least a few hundreds. However, in our case the basis cell of the crystal only contains a few particles, therefore we have also to take into account at least a few neighbouring cells in the real sum. We can not first set R_{max}=0 or 1 and then search the ν for which the terms of the real space sum with $R > R_{max}$ are negligible, because such a ν does not exist. In this case, ν has to be chosen first.

3.5. Choice of ν

To find an appropriate value for ν [23], large values of R_{max} and k_{max} (e.g 50 and 50) are assured and a configuration (lattice parameters of the unit cell, position of the basis particles) is fixed. ν is varied from 1 to 12 in small steps, and for each step the energy of the configuration is calculated. If the energy of the configuration versus ν is drawn (see figure 3.2), a plateau can be observed for which the energy is independent of ν. A divergence of the curve at small ν is due to the non convergence in the real space sum, while a divergence of the curve at large ν is due to the non convergence in the reciprocal space sum. This procedure is repeated for different configurations, then a ν is chosen which is in the plateau of each configuration.

The divergence of the energy takes mainly place at large ν. A very small value of ν could also be chosen, but this would force the choice of a large value of R_{max}, which is to avoid since the calculation in the real space is slower than in the reciprocal space (see figure 3.3). The value of ν chosen is therefore the largest one which is in the plateau of all configurations tested - or a bit smaller to keep a security margin because the set of configurations chosen may not be perfectly representative of the whole set of possible configurations.

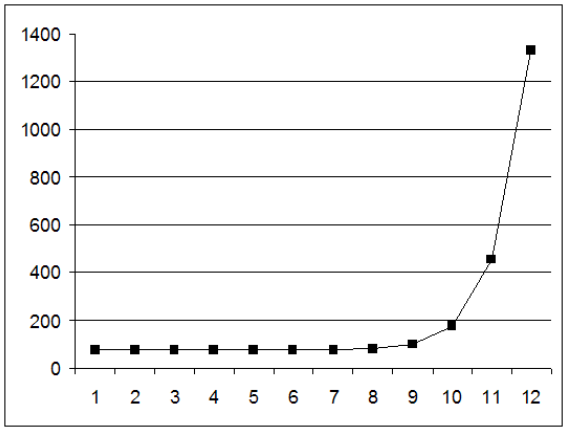

Figure 3.2.: Energy of a chosen configuration as a function of ν, with large values of R_{max} and k_{max}. After a plateau the energy diverges.

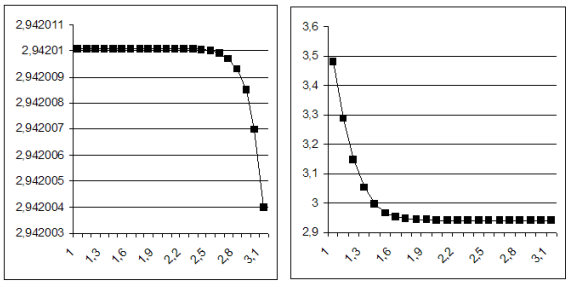

Figure 3.3.: Energy of a chosen configuration as a function of ν. Left $k_{max} = R_{max} = 12$, right $k_{max} = 12$ and $R_{max} = 1$ (the same graph is obtained with $k_{max} = 30$). It can be seen right that if one wants to choose a very small ν, e.g. 1.3, R_{max} can not be chosen equal to 1 because for (R_{max}=1, k_{max}=12, ν=1.3) the energy is not in the plateau. For R_{max} bigger (left), ν can be chosen very small, but a large R_{max} is not wished. ν will thus be chosen so that the energy still is in the plateau for small values of R_{max}. ν=2 for example is a possible choice for this configuration.

3.6. Choice of R_{max} and k_{max} [23]

Once the value of ν fixed, the search for k_{max} and R_{max} can begin. These searches are independent from each other, thus one can equally well start off with either one or the other.

For example, one begins with the search for the optimal value of k_{max}. R_{max} is set to a high value, ν to the value found in the previous step, and a configuration is chosen. The energy plotted as a function of R_{max} shows a plateau from a particular R_{max} value onwards. However, in contrast to the previous step, this plateau is maintained as R_{max} increases: the R_{max} for which the plateau begins is such that all terms of the real space sum with $R > R_{max}$ are negligible, and so the energy stays constant when these terms are added. This operation is repeated with other configurations; the value of R_{max} chosen afterwards is the smallest one among those which are in the plateau of each configuration. Thus no term with an relevant contribution to the real space sum is omitted. A larger value of R_{max} could be chosen, the energy would always be correct, but useless calculations would be performed.

The same procedure is repeated, keeping ν and k_{max} fixed at those values that were found previously, and R_{max} being varied.

The same values for k_{max} and R_{max} can be chosen for all lattice directions, or one can choose individual values for each direction: $R_{max,a}$, $R_{max,b}$, R_{max}, and $k_{max,a}$, $k_{max,b}$, $k_{max,c}$, which might help to avoid useless calculations. If the same value is chosen for all the directions, it has to be $R_{max} = \max(R_{max,a}, R_{max,b}, R_{max,c})$ and $k_{max} = \max(k_{max,a}, k_{max,b}, k_{max,c})$ to ensure the accuracy of the result.

One risk of this method is that the chosen configurations may not be representative of the whole set of configurations for which the energy will have to be computed.

3.7. Speeding up the calculation

3.7.1. Two problems of the Ewald summation

The first problem in the Ewald summation is that it is computationally demanding, since one part of the problem is solved in the reciprocal space where several Fourier transformations are needed.

Furthermore, for this method, the computer time scales with the number of particles as N^2, or in the best versions as $N^{3/2}$ if the used cut offs are optimized with respect to the splitting parameter [24]. This second problem is a serious one for the molecular dynamics simulations, where the number of particles in the simulation box is very large. For the case studied here this problem is less relevant since there are only a few particles in the basis cell. However, as seen previously, owing to this small number of particles the real part sum can not be truncated at $R = 0$. This will prevent a considerable speed-up of the calculation since the improvements mainly take place in the reciprocal space sum.

3.7.2. Some solutions

Tabulation

The first problem can be tackled by tabulating the complete Ewald potential (in our case the Stockmayer potential) as a function of the distance between two particles and then performing polynomial approximations [25, 22]. For this approach to be feasible and sufficently accurate, the interpolation method used must be rather simple and the table has to be 'moderately' fine [26, 25]. The risk is indeed to loose accuracy in the energy value.

However, this approach does not solve the second problem and in addition, interpolation in combination with forward/backward transformations may lead to serious computational costs. Alternatively, one can tabulate only the direct space sum, provided that the reciprocal-space sum can be computed efficiently, or only the exponential and/or the complementary error function erfc which are part of the potential (see appendix B.1). Tests showed that in certain cases the speedup is about 50% when the table look-up is used for both the exponential and the complementary error function [26]. Tables also enable to calculate the numerical derivative of a function. For example $\exp(-x^2)$ is obtained for free when $\mathrm{erfc}(x)$ is tabulated since $\frac{\mathrm{d}}{\mathrm{d}x}\,\mathrm{erfc}(x) = \frac{-2}{\sqrt{\pi}}\exp\left(-x^2\right)$.

In summary, tabulation methods attempt to establish a balance between accuracy versus speed, a trade-off that is dependent on the size of the system and the objective of the calculation. These methods can produce a major impact in speeding up MD/MC applications where medium accuracy is acceptable. Higher accuracy simulations with tabulation may suffer in performance due to low resolution in coarse

tabulation and/or expensive interpolation, or run out of storage for high-resolution tables [26].

Polynomial approximation methods [26]

This approach attempts to improve the accuracy and performance of the Ewald sum calculation by using a polynomial approximation rather than tabulation. The idea is to find a polynomial approximation to the Ewald potential that is cheaper to evaluate and then differentiate it analytically to get the forces.

Factorisation

The reciprocal space sum of the dipolar potential can be factorized (see appendix B.1.1):

$$U_{DF} = \frac{1}{2}\sum_{i=1}^{N}\sum_{j=1}^{N}\sum_{\mathbf{k}\neq 0}\frac{1}{\pi V_c}(\boldsymbol{\mu}_i\cdot\mathbf{k})(\boldsymbol{\mu}_j\cdot\mathbf{k})(4\pi^2/k^2)\exp(-k^2/4\nu^2)cos(\mathbf{k}\cdot\mathbf{r}_{ij}) \tag{3.5}$$

$$= \frac{2\pi}{V_c}\sum_{\mathbf{k}\neq 0}\frac{1}{k^2}\exp(-k^2/4\nu^2)\tilde{M}(\mathbf{k})\tilde{M}^*(\mathbf{k}) \tag{3.6}$$

with

$$M(\mathbf{k}) = \sum_{i=1}^{N}(\boldsymbol{\mu}_i\cdot\mathbf{k})\exp(-i\mathbf{k}\cdot\mathbf{r}_i) \tag{3.7}$$

$$= [(\boldsymbol{\mu}_i\cdot\mathbf{k})\cos(\mathbf{k}\cdot\mathbf{r}_i) - i(\boldsymbol{\mu}_i\cdot\mathbf{k})\sin(\mathbf{k}\cdot\mathbf{r}_i)] \tag{3.8}$$

$$\equiv \Re(\tilde{M}(\mathbf{k})) - i\Im(\tilde{M}(\mathbf{k})) \tag{3.9}$$

This manipulation has transformed the double sum over i and j, which is of order N^2, into a single sum over i in $\tilde{M}(\mathbf{k})$. This sum is of order N and therefore much more efficient [26, 15].

Further truncation schemes

In addition to the truncation of the sums in the real and the reciprocal space at R_{max} and k_{max}, spherical cutoffs can be used for rapidly decreasing functions in order to avoid the calculation of negligible contributions. The spherical cutoff radius is determined for each function by the accuracy desired: the accuracy of the result, but also the computational time, increase with the radius [26].

Neglecting the contribution of the reciprocal space

To speed up a MD simulation, Rycerz and Jacobs [27] suggested that by properly choosing the simulation parameters, the reciprocal-space sum contribution to the total energy can be neglected entirely. For MD simulations of Bi_2O_3 performed with 270 particles and with 2160 particles, choosing $\nu = 5.6/L$, and using the minimum image convention, the authors estimated the reciprocal-space contribution to the potential energy to be about 1:1500. Similar observations were made for a crystalline and molten NaCl system [27]. It was pointed out [27] however, that this approach should not be applied to small systems as the energy becomes strongly dependent on the system's configuration. Moreover, there is no indication that other ionic systems will have similar small contribution to the energy. It is also unclear whether the method can be extended to polar systems. Therefore, this method requires more investigations and is currently limited to large ionic systems. It can not be applied for the present case.

3.7.3. Extensions and alternatives to the Ewald summation

The P^3Mesh method (i.e particle-particle/particle mesh method) of Eastwood and Hockney [28] scales like $N \log(N) \sim N$. Here, the evaluation of the implicit Fourier transform present in the reciprocal space terms is done trough the use of the fast Fourier transform technique (FFT), which reduces substantially the time needed to compute the reciprocal space sum. Other methods speeding up the calculation are the Fast Multipole Method [29], which scales as $O(N)$, the Lenkner sum, the MMM method [30]. However, these $O(N)$ algorithms [28, 29] only become more efficient than the Ewald summation for systems containing on the order of 10^5 particles. For intermediate size ($N \sim 10^3 - 10^4$) the so-called particle-mesh Ewald (PME) summation [31] is an attractive alternative. This method is declined in another version: the smooth PME [24].

A complete different method from the physical point of view but also very useful to compute long-range interactions is the reaction field method [18], which assumes that the interaction from particles beyond a cutoff distance can be handed in an average way.

4. Genetic algorithms

Genetic algorithms are an optimisation tool based on ideas of Darwin's theory of evolution [32]. They were probably first introduced by J. H. Holland [11] in 1975. They have then been developed [33, 34, 35] and, turning out to be robust, reliable, powerful, adapted for problems in large and complex search spaces (where random search is not possible) and of rather simple implementation, they were applied in very different domains such as biology [36], economics [37, 38], finance (forecasting stock market prices and foreign exchange), automated design [39], timetabling problems, the traveling salesman problem, criminal identification, physics, chemistry and material science [40, 41, 42].

In our group, they have been successfully used for identifying ordered equilibrium structures in condensed matter [43, 44], 3D soft matter systems [45, 46, 47, 48], 2D soft matter systems [49, 50, 51, 48] and 2D soft matter layered systems [52].

For the present study they will be used to find the ordered structures of the Stockmayer system.

4.1. Difficulties for identifying material structure

The traditional way of identifying crystal structure is based on experiment, which requires to synthesize the material and to study it under suitable conditions. The employed method is often cumbersome.

A theoretical prediction can be done by listing all the lattices that we think could be the one of the sample studied and then computing their energy. The most stable structure, i.e. the one with the lowest energy, is the most plausible candidate for the sample structure. However, this method is biased: some structures might have been omitted during the elaboration of the list, a choice which is based on experience, intuition or plausible arguments. The solution found is the most plausible among

the structures studied, but some more stable structures may have been forgotten.

On the other hand, genetic algorithms are an unbiased optimization tool which performs the search in the whole parameter space. These two features represent two big advantages of genetic algorithms with respect to other optimization tools.

The minimization of the energy with respect to all possible lattices with the help of genetic algorithms is far from trivial because of the following reasons [53]:

- the search space is high dimensional: five degrees of freedom per particles ($x_{\text{center}}, y_{\text{center}}, z_{\text{center}}$ plus θ and ψ for the dipole orientation) and six additional degrees of freedom for the lattice ($\|a\|, \|b\|, \|c\|, \alpha, \beta, \gamma$). One particle can be fixed at the corner of the basis cell, so that the total dimension of the space is given by 6+5N-3. But in some parts of the genetic algorithm, the lattice is coded trough the 3x3 Cartesian coordinates of its lattice vectors and all the parameters are allowed to vary independently: the dimension of the search space is then 5N+9.
- The energy surface is rugged, i.e. the energy may changes drastically with a little change of one of the parameters.
- Different unit cells can describe the same lattice structure. All unit cells describing the same lattice structure are equivalent to a unique basis cell with the following properties:
  - the angles $[\alpha, \beta, \gamma]$ are in [60°,120°],
  - the lattice vector $\mathbf{a}$ is in the same direction as $\hat{\mathbf{e}}_x$,
  - one particle is at the origin O (0,0,0).
- An accurate calculation of the energy is computationally expensive, as seen in the precedent chapter. However, calculations of high numerical accuracy are indispensible since the relative energy difference between two competing structures, fcc and hcp for example, can be of the order of $10^{-5} - 10^{-6}$.

4.2. Basic ideas of a genetic algorithm

In an evolutionary (often called genetic) algorithm, a set of possible structures is randomly chosen. Based on selection, cross-over, mutation and relaxation operations (see 4.3), these structures pass an artificial evolution. The selection operation chooses

stable structures to be kept for the next step, the cross-over operation generates new structures, the mutation operation introduces random variations to find new solutions and the relaxation operation optimizes locally the structures in the parameter space.

4.2.1. Encoding the structures

Essentially two solutions exist to encode the structures, namely the genotype and the phenotype algorithms, distinguishing between two sorts of evolutionary algorithms. The genetic (genotype) algorithms code the lattice and particles parameters with the binary alphabet (see fig.4.1). The name of the algorithm comes from the ressemblance to sequences of genes. On the other hand, the phenotype algorithms directly use the real values of the parameters of the structure (the phenotype) [54]. However algorithms of this last type are still often called "genetic algorithms" in most scientific contributions.

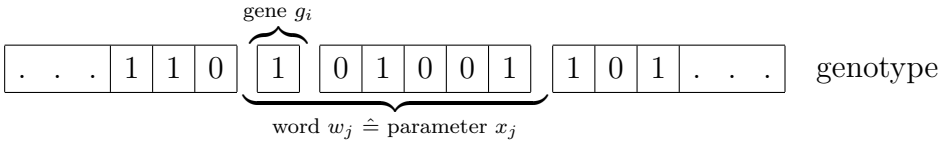

Figure 4.1.: Coding of the structures in genetic algorithms. What is refered to as "gene" in these algorithms rather corresponds to the "allele" of a gene in biological genetics. [48]

In this thesis we will use a phenotype algorithm.

4.2.2. Vocabulary of evolutionary algorithms

A possible structure is called an individual, and the set of possible structures at a certain time is called a generation or a population, depending of the context. The initial generation is randomly created, then its individuals undergo a set of operations which creates the individuals of the next generation. An individual is given by the lattice parameters of its basis cell plus a certain number of particles defined by their position within the basis cell and the orientation of their dipoles.

The evaluation function of an individual, i.e. the function evaluating its quality, is in our case the Gibbs free energy (G). This evaluation function has to be minimized:

the lower G, the higher the quality of the individual.

The fitness of an individual is a function of its quality: the higher the quality is (i.e. the lower the energy is), the higher the fitness function is. Different functions can be used as fitness functions [48, 44], depending on which weight one wants to give to the individuals of high quality and to those of lower quality. If the selection is too strong, good individuals are by far preferred and propagate very fast: the diversity of the population decreases and the risk of convergence towards a local minimum is large. On the other hand, if the selection is too weak, good individuals are hardly preferred and the algorithm converges really slowly or not at all; the evolutionary algorithm becomes a random search. A good choice of fitness function (the quality of the choice depending on the studied system) can economize a large part of the computationnal effort [44].

Some examples of fitness functions [48] are:

- **Proportional fitness:** $f_{\text{prop}}(I) = aG(I)/\sum_J G(J)$ with
  - a a parameter;
  - $f(I)$ the fitness value of the individual I;
  - $G(I)$ the Gibbs free energy of the individual I;
  - the sum extending over all individuals in the population.
- **Linear fitness:** $f_{\text{lin}}(I) = L(G(I))$, where L is a linear function on $\mathbb{R}$.
- **Exponential fitness:** $f(I) = \exp\left(-a\frac{G(I)-\min(G)}{\max(G)-\min(G)}\right)$, with
  - a a positive parameter;
  - $\min(G)$ and $\max(G)$ the minimal and maximal values of the Gibbs free energy among the individuals of the generation.

We chose as fitness function in our algorithm an exponential fitness function of parameter $a = 3$.

4.2.3. Simplified phenotype algorithm

The framework of a phenotype algorithm can be represented as follows where variables are typed in `roman` and operations in *`italic`* letters [48]:

```
program GA
  initialize(population)
  evaluate(population)
  while (not(termination_condition)) do
    parents=select_parents(population)
    new_generation=recombine(parents)
    new_generation=mutate(new_generation)
    new_generation=relaxe(new_generation)
    evaluate(new_generation)
  end do
end program
```

4.3. Principal parts of the phenotype algorithm

4.3.1. Initialisation

During the initialisation, a population of individuals is randomly created. The number of individual as well as the volume of their basis cell, V_{uc}, is given as input. The lattice angles α, β and γ are randomly chosen between 60° and 120° and the lengths of the lattice vectors are also randomly chosen. The basis cell is then rescaled so that its volume equals the given volume V_{uc}. The particles are placed randomly in the unit cell - we do not place a priori a particle at the origin. The individual is then relaxed and undergoes a strict control as we will see below (see 4.3.2).

The random initial population can be replaced by a population given by the user, if some intuitive result is available. Furthermore, if some parameters are known, for example if the lattice parameters are available from an experiment, they can be fixed as constant during the whole search [44]. This reduces the space search significantly, but can completely misdirect the search by favourising a local minimum. Therefore, this technique has to be implemented carefully [53].

4.3.2. Improvement of a given population

The following operations take place as well at the end of the initialisation, after the creation of a random population, as at the end of the reproduction procedure, i.e. after the creation of a following generation.

Relaxation

The relaxation operation is a local optimization operation of an individual. Evolutionary algorithms are global optimization methods; they provide a serious candidate for the basis cell of the structure, which can be refined with the help of a local optimization. As the fitness value can change very strongly for an individual before and after the local optimization, this operation is really necessary [53].

Several local optimization methods have been proposed in literature [55, 56], for example the steepest descent conjugate gradient methods [53] or the hill-climbing search; in our work we use the L-BFGS-B method. The L-BFGS acronym stands for Low-memory Broyden-Fletcher-Goldfarb-Shanno quasi-Newtonian minimizer. This method is often used to solve unconstrained non-linear optimization problems and is the standard method for cluster-geometry optimzing phenotype algorithms [57, 58]. The L-BFGS-B method is a further development of the L-BFGS method allowing to introduce bounds (maximal and minimal values, but no general constraints) on the variables [59, 60].

The L-BFGS-B method approximates an inverse Hessian matrix from previous configurations [61]. The gradient of the energy with respect to the variables is calculated, providing the direction towards the minimum of the energy. The variables are of three kinds: the lattice parameters, the fractional coordinates of the particles and the orientation of the dipoles. The lattice is parameterized by the Cartesian coordinates of the lattice vectors: $(a_x, a_y, a_z, b_x, b_y, b_z, c_x, c_y, c_z)$, that is, nine parameters. The fractional coordinates (x_f, y_f, z_f) of the particles are their position in the basis cell (see Appendix A).

The dipole orientation is given by the two angles of the spherical coordinates θ and ψ. Altogether, the energy is locally minimized according to $9 + 5N$ parameters with N the number of particles in the basis cell.

Once the gradient is computed, the individual is replaced by the one that have been obtained by minimizing the energy. The procedure is repeated (calculation

of the energy and of the gradient of the individual), until a local minimum of the energy is reached. In this process, the gradient with respect to the variables has to be calculated many times, an operation which requires large computational costs. Fortunately the precision required for the gradient of the energy is not as high as for the energy itself; in our work we limited the accuracy to a few percents.

This method is really powerful. For a phenotype algorithms, considering a few particles per basis cell, it allows to find the best solution for the material structure within a few generations. The relaxation is the most time consuming part of the algorithm. The number of individuals per generation must then be limited (between 4 and 20, for example) for the calculation to be made in a reasonable time [35].

Population control

This function permits to accelerate the convergence of the algorithm by rejecting individuals with bad geometric properties and by avoiding energy niches. Use of this function is optional.

As 'individuals with bad geometric properties' we understand individuals characterized via at least one of these two criteria:

- the lattice angles lie far outside the interval [60°,120°] (since all structures can be described by a unit cell with lattice angles in [60°,120°], those individuals are redundant),

- individuals which have unphysical lenghts (lenght of a lattice vector or distance between two particles smaller than σ, the diameter of a particle).

If some other properties of the system are known, they can be included in these tests.

Avoiding energy niches means that all the individuals of the population should not have their energy within the same small interval: the difference between the energies of two individuals should be larger than 5.10^{-3}. This step helps to avoid that the individuals are not all located around a local energy minimum, ignoring a global minimum with a quite different structure.

4.3.3. Reproduction

Once the initialisation is finished, the reproduction can take place. It consists in creating a new generation from the old one, with the same number of individuals. It consists of three steps: selection, cross-over and mutation.

Selection

A certain number of individuals of high quality is taken from the previous generation, without any changes: this is called the elitism. This fixed number of individuals is given as an input. It ensures that the energy of the best individual of the generation decreases monotonically from generation to generation since at least the best individual of the old generation is copied to the new generation. The other individuals of the new generation are created from two individuals of the old generation, the parents. The choice of the parents is made with the help of the fitness function. Since individuals with higher fitness values have more chances to be selected, the average fitness value of the generation produced should be higher than the one of the parent generation. Different selection strategies are possible [48]:

- *linear ranking*: all potential parents, i.e. the individuals of the old generation, are sorted in term of their fitness value. They receive a selection probability which decreases when the ranking diminishes. As this probability only depends on their rank and not on the value of their fitness, this method prevents domination of individuals with a very high fitness value.
- *tournament*: a number n of potential parents is randomly selected and the individual with the highest fitness value in this selection is kept as a parent. The same procedure is repeated to find the second parent of the new individual. The higher n is, the smaller the chance of individuals with a low fitness value to be selected is.
- *roulette wheel*: the selection probability of an individual is proportional to its fitness value as if a roulette wheel was used, with the slot width corresponding to each individual proportional to its fitness value. It is one of the most popular selection method and the one which we have used in our algorithm.

The individuals of the old generation selected as parents for a child individual are not removed from the population and can thus be selected mutiple times. However, the two parents of a child individual have to be different.

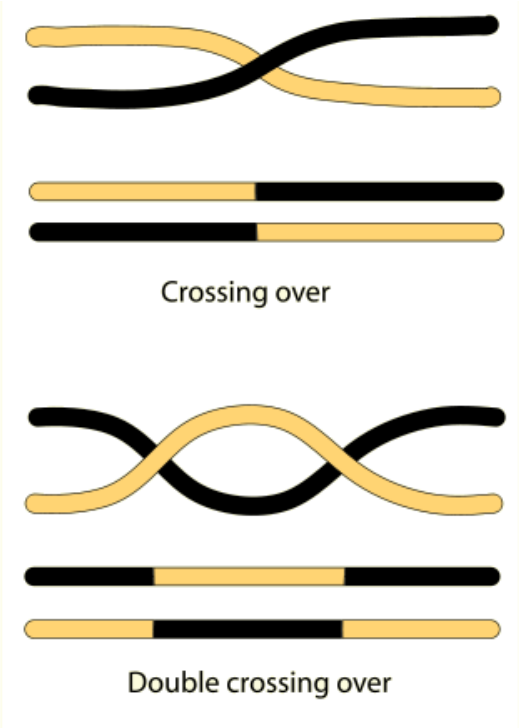

Figure 4.2.: Scheme of a one-point and a two-point cross-over

Cross-over

To create a new individual from the two parents determinated in the previous step, the cross-over (or crossing over) technique is used. In the genetic algorithms, as in the biological analogue, the gene string of each parent is cut at the same, randomly chosen, position. One child gene string is obtained by taking the left side of the gene string of the first parent and the right side of the one of the second parent (see fig.4.2). The other child string is obtained by taking the right side of the gene string of the first parent and the left side of the one of the second parent. A two-point crossover can also happen (see fig.4.2), with two cut sites and where the middle of the gene string is taken from one parent and the extremities from the other one. For the algorithm the method of the uniform crossover can also be used: each bit of the gene string of the child is randomly taken either from the corresponding one in the first parent gene string or from the the corresponding one in the second parent gene string.

For the phenotype algorithms, the crossover does not take place with the genes but with the position and orientation of the particles and with the lattice parameters.

To begin with, the basis cells of the parents are reorientated: the coordinates x and y, x and z or y and z of the lattice vectors and of the particles are exchanged.

The particles of both individuals can then be shifted along the lattice vectors. For each individual and each vector along which to be shifted, a random number is generated and added to the respective coordinates. Since the basis cell is periodically repeated, a particle that ends up after this operation outside the cell is replaced by its periodic image particle inside the basis cell. The system is not physically changed by the procedure but this operation increases the diversity of the individuals and can therefore enhance the power of the algorithm. The probability of shifting, which can be different for the different lattice vectors, can be fixed by the user. Typically nearly 100% of moves in the direction along which the cross-over will take place (see below) and around 5% of moves in the two other directions is efficient [53].

Each lattice parameter of the child individual is obtained from a linear combination of the corresponding lattice parameters of the two parents with random weights. The random weights are different for each lattice parameter. For the particle cross-over, the particles of the parents are ordered according to their coordinates along a randomly chosen Cartesian direction: this will be the direction along which the cross-over will take place. An integer number n between 0 and N, the number of particles per individual, is then randomly produced. The child individual is formed by the n first particles of the first parent (first particles in the new order) and by the last (always in the new order) $N - n$ particles of the second parent. The particles are copied from the parents with their fractional coordinates and the respective orientation of their dipole.

An alternative method for the particle cross-over is to produce a random number $x \in [0, 1]$ and to compose the child with all the particles of the first parent which have a coordinate along the cross-over direction smaller than x and all the particles of the second parent which have a coordinate along the cross-over direction larger than x. This corresponds to a cut of both parent cells by a plane parallel to the plane spanned by the two lattice vectors others than the cross-over axis vector. With this method, the child may not have the same number of particles as its parents ; this new individual has to be adjusted to reach the correct number of particles [53].

Mutation

In order to avoid the attraction of a local minimum in the energy landscape, mutations are randomly introduced on the individuals. Two types of mutation exist: mutation of the lattice, where the lattice parameters are randomly changed, and mutation of the particles, where their coordinates and the orientation of their dipole are randomized. Only a small, random number of lattices and particles undergo these transformations. The probabilities of mutation are given by the mutation rates, input parameters of the algorithm. They can also increase with the number of generations. Their value is rather small, usually between 0.001 and 0.1.

The mutation of the lattice consists in applying a symmetric strain matrix to the matrix composed with the Cartesian coordinates of the lattice. The new lattice vectors **a'**, **b'** and **c'** are obtained via

$$\begin{pmatrix} a'_x & a'_y & a'_z \\ b'_x & b'_y & b'_z \\ c'_x & c'_y & c'_z \end{pmatrix} = (I + \boldsymbol{\epsilon}_{ij}) \begin{pmatrix} a_x & a_y & a_z \\ b_x & b_y & b_z \\ c_x & c_y & c_z \end{pmatrix} \tag{4.1}$$

where I is the identity matrix and $\boldsymbol{\epsilon}_{ij}$ the strain matrix :

$$\boldsymbol{\epsilon}_{ij} = \begin{pmatrix} 1+\epsilon_{11} & \frac{\epsilon_{12}}{2} & \frac{\epsilon_{13}}{2} \\ \frac{\epsilon_{12}}{2} & 1+\epsilon_{22} & \frac{\epsilon_{23}}{2} \\ \frac{\epsilon_{13}}{2} & \frac{\epsilon_{23}}{2} & 1+\epsilon_{33} \end{pmatrix} \tag{4.2}$$

where the ϵ_{ij} are Gaussian random variables with zero mean value [53].

The mutation of the particles consists in adding zero mean Gaussian random variables to their coordinates [53].

The mutation of the lattice is important firstly to prevent the algorithm to converge too fast towards a particular structure which might be only a local minimum and secondly to explore the neighbourhood of an individual of good quality. On the other hand, the mutation of the particles is not essential because of the diversity already achieved through the heredity and the local optimization [53]. We have not implemented this second mutation procedure in our algorithm.

Termination of the reproduction

If the crystal consists of different types of particles, some particles of different kinds can be permutated in order to facilitate the correct ordering of particles. We will

only consider structures with one type of atoms, that's why we will not use this procedure.

All the individuals of the new generation are rescaled to the volume V_{uc} given by the precedent generation. The newly created population undergoes then the improvement operations described in 4.3.2. A new V_{uc}, which will be used for the next generation, is then calculated. It is an average between the old value of V_{uc}, from the parent generation, and the average of the volumes of the best individuals of the child generation. The volume of the individuals of the child generation is indeed no more V_{uc}, because it has been changed during the relaxation. Depending on the weight given to the previous V_{uc} and to the volume of the best individuals of the child generation, the volume V_{uc} converges more or less fast to its value permitting the lowest Gibbs free energy.

4.3.4. Input/output

The input file contains the parameters fixed by the user of the algorithm, particularly:

- physical parameters:
  - the number of particles per basis cell,
  - the absolute value of the dipole,
  - the pressure;
- parameters of the algorithm:
  - V_{uc}, the volume per particle for the individuals of the initial generation,
  - the number of individuals per generation,
  - the number of generations that are created: the algorithm terminates when the given number of generations is reached,
  - the mutation rates of the lattice and of the particles,
  - the elitism, i.e. the number of individuals of the parent generation being copied as they are to the child generation. If the initial generation is not a random one but is composed of structures which are thought to be good solutions, the elitism is chosen higher than in the case of a random initial generation.

The output consists in the individual of the lowest energy reached during the whole calculation. Its energy is given as well as its lattice parameters, the position of its particles and the orientation of their dipole. The volume of the basis cell and the density of the structure, for example, can also be given.

5. Implementation of the phenotype algorithm and results

Our phenotype algorithm is programmed in FORTRAN 90 and uses two external packages, namely *RANLUX*, a pseudo-random number generator proposed by M. Lüscher [62, 63] and *TOMS778* [64], a FORTRAN 90 implementation of L-BFGS-B for local optimization purposes. For the calculation of the Lennard-Jones energy via Ewald sums (see eq.B.21), we adapted a programme calculating the incomplete gamma function [65] and for the calculation of the dipolar contribution to the energy and the related forces we adapted a programm of M. P. Allen and D. J. Tildesley helping for the factorization of the dipolar energy and of the related forces and for the tabulation of parts of the potential (see 5.1)[66]. Our algorithm strongly relies on a phenotype algorithm developed by Günther Doppelbauer [48], which is based on a genetic algorithm implementation written by Dieter Gottwald [43] and improved by Julia Fornleitner and Gernot Pauschenwein [49, 45].

The programme is controlled via an input file of the following kind.

PARTICLES 2

INDIVIDUALS 6

GENERATIONS 20

MUTATIONRATE 0.01

FITNESSPARAMETER 3

ELITISM 2

MOMENT 4

INITIAL_V_UC 1.0

PRESSURE 20

5.1. Parameters of the Ewald sums

In the following, σ and ϵ are fixed for simplicity as lenght and energy units. We have then $\mu = m^*$ and $\rho = \rho^*$ (see 2.4).

For the Ewald summation for the Stockmayer potential, the numerical parameters ν, R_{max} and k_{max} have to be fixed. With the help of the method described in 3.5 and 3.6, we have used ν=1.3, R_{max}=7 and k_{max}=12. These values guarantee for a relative accuracy of 10^{-6} in the energy. The set of possible configurations used for the determination of these values has been preselected by the following criteria: the distance between the particles is not a lot smaller than σ and the volume per particle has to lie in the interval $[0.5\sigma^3, 2\sigma^3]$. We have then verified that during the run, the volume of the individuals remains in the neighbourhood of this interval to ensure the desired precision. To compute the forces, the same value of ν as for the energy evaluation is kept; however, in order to guarantee the same numerical precision for the forces as the one for the energy, the values of R_{max} and k_{max} have to be very large - up to 70. Such a choice of numerical parameters would lead to a too long computation. We therefore lowered the desired numeric precision of the forces to a few percents, which is enough for the relaxation procedure to work correctly. R_{max}=2 and k_{max}=12 are then sufficient for the Lennard-Jones forces, and R_{max}=5 and k_{max}=10 for the dipolar forces.

5.2. Speeding up the calculation

We used the factorization described in 3.7.2 to accelerate the calculation of the energy and of F_{DF} (see Appendix A for the notations). In this purpose, we tabulated the factors $e^{i\mathbf{k}\cdot\mathbf{r}}$ for all particles and all $\mathbf{k}$-vectors. Futhermore, we tabulated the factors $2\pi e^{\frac{-k^2}{4\nu^2}}/k^2$ for all $\mathbf{k}$-vectors. These operations have to be done for each new individual and each time that the individual changes, during the relaxation operation for example, because the positions of the particles and the lattice vectors - and thus the reciprocal vectors - change. These operations are adapted from the ones presented by Allen and Tidesley in [66].

Even after these measures, the required computational time of the algorithm was still too high for a practical use. Three quarters of the CPU time were used to compute the incomplete Gamma function, part of the Lennard-Jones contribution to the

energy and of the associated forces. Further the exponential function and the complementary error function, both required for the dipolar contribution to the energy and for the associated forces, also needed a non negligeable time to be computed. We thus tabulated the incomplete gamma function, the exponential function and the complementary error function at the beginning of the algorithm. In contrast to the previously mentioned functions, these functions are not tabulated for each wavevector and each real vector that are used in the programme, but on equally space grids in r and k, varying from 0 to a cut off value, beyond which the tabulated functions are negligeable. This tabulation requires an interpolation scheme (as described in 3.7.2) to compute the value of the functions for the r and k vectors which are not in the table, introducing hereby approximations. We chose the cut off values such that for the values of the variables larger than the cut off, the value of the function was smaller than 2.10^{-12}. While the approximations due to the interpolation scheme introduced numerical errors that were still too large to guarantee the desired precision of 10^{-6} in the energy, the achieved numerical precision in the forces was sufficient, thus we used in the following the tabulation of the incomplete gamma function, of the exponential function and of the complementary error function to compute the forces but not to compute the energy. For the calculation of the energy, we only used the same cut off values as for the tabulation, i. e. we set the function equal to zero when its variable was greater than its cut off value. The desired accuracy was guaranteed and the computation speeded up.

The calculation of the incomplete Gamma function still needed too much computational time. Since the Lennard-Jones potential is short-ranged, we tried to implement the direct sum (full computation taking place in real space) of the Lennard-Jones energy and forces to solve this problem. To obtain the desired accuracy in the energy, we had to assure $R_{max} = 300$, which even increased the computational time. However for the desired accuracy for the forces, $R_{max} = 5$ was sufficient. We then decided to compute the Lennard-Jones energy with the Ewald sum and the Lennard-Jones forces with the direct sum, so that the tabulation of the incomplete Gamma function was not needed anymore.

The population control procedure was finally not implemented because the relaxation was "too" efficient in the following sense: if an individual was discarded for one or another reason, a new individual was produced; however the relaxation of this last individual ended in an individual very similar to the one which had been discarded. Thus this new individual had to be discarded for the same reason, etc.. Since the population control finally needed a too large amount of time and sometimes hindered

the convergence of the algorithm, we did not activate it.

5.3. Results

We studied a system of dipolar particles interacting via the Stockmayer potential with all the dipoles being parallel to the z direction, similar to the investigations of B. Groh and S. Dietrich [2]. We varied the absolute dipole value μ from 0 to 12 and the pressure P from 0 to 500 in units of ϵ/σ^3. For each state point, characterized by a pair (μ, P), we searched for the crystal structure with the minimal Gibbs free energy. For this purpose, we ran the algorithm varying the number of particles in the basis cell from 1 to 9. For each number of particles, μ and P being fixed, three independant runs of the programme were performed; from the three results we kept the one with the lowest Gibbs free energy. The best structure for a given couple (μ, P) is then determined by comparing the results obtained for these values of μ and P and the different numbers of particles. The structure with the lowest Gibbs free energy is retained. It is necessary to run the algorithm with different numbers of particles in the basis cell because for example the hcp structure, whose minimal unit cell contains two particles, can equivalently be described by an n-times larger basis cell of $2n$ particles and so can be reached by the algorithm when the number of particles in the basis cell is a multiple of two, but not for three or five particles. It is also a reliable test for the algorithm: if this one is reliable, one should obtain exactly the same structure for each multiple of the number of particles in the minimal basis cell of the stablest structure. Running the algorithm with a number of particles in the basis cell up to nine allows us to assure that there is no structure with, for example, seven particles in the basis cell which has a lower Gibbs free energy than the one we found. Structures with more than nine particles in their basis cell are unlikely. In each run, we considered between 20 and 50 generations - 20 for a small number of particles, 50 for the larger numbers of particles per unit cell.

In our work — similar as in [53] — , the correct structure prediction was usually achieved in a few runs. With a few particles per cell, the global minimum was found by the local optimization (relaxation procedure). However, this is not the case for all the systems: with more complex systems like molecular ones, more generations would have been needed [53].

Once the individual with the lowest energy for a given state point found, we inden-

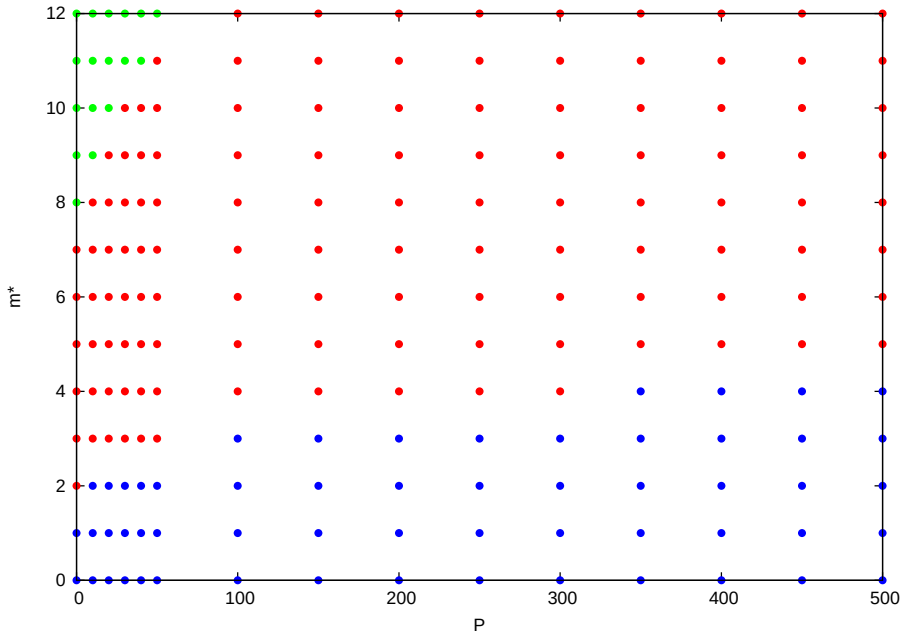

Figure 5.1.: Identified ordered structures for the Stockmayer system in the (m^*, P)-plane. Symbols: red-bco, green-bct and blue-hexc. When P tends to zero, hexc reduces to hcp.

tified its crystal structure with the program *FINDSYM* developed by H. T. Stokes and D. M. Hatch [67] and the website of the Center for Computational Materials Science of the US Navy [68]. The structures were then visualized with the software *PYMOL* [69].

The obtained structures are hcp, hexc, bco and bct as shown in fig.5.1. For the description of these structures, see Appendix C. When the absolute value of the dipole increases, the length of the c axis decreases. For $P = 0$ and $m^* = 0$ for example, the hcp structure, which has two particles in its simplest basis cell, was found when the number of particles in the basis cell of the individuals in the algorithm was 2, 4, 6 and 8, but not for 1, 3, 5, 7 and 9.

When minimizing the Gibbs free energy, we obtained the equilibrium density as a result for a particular state point. These values could then be compared to those of B. Groh and S. Dietrich [2], who searched for the structures with the minimal energy for given values of m^* and ρ^* (see fig.5.2).

For $m^* = 0$, that is to say, when the Stockmayer potential is reduced to the Lennard-Jones potential, we found that the structure with the minimal Gibbs free energy is

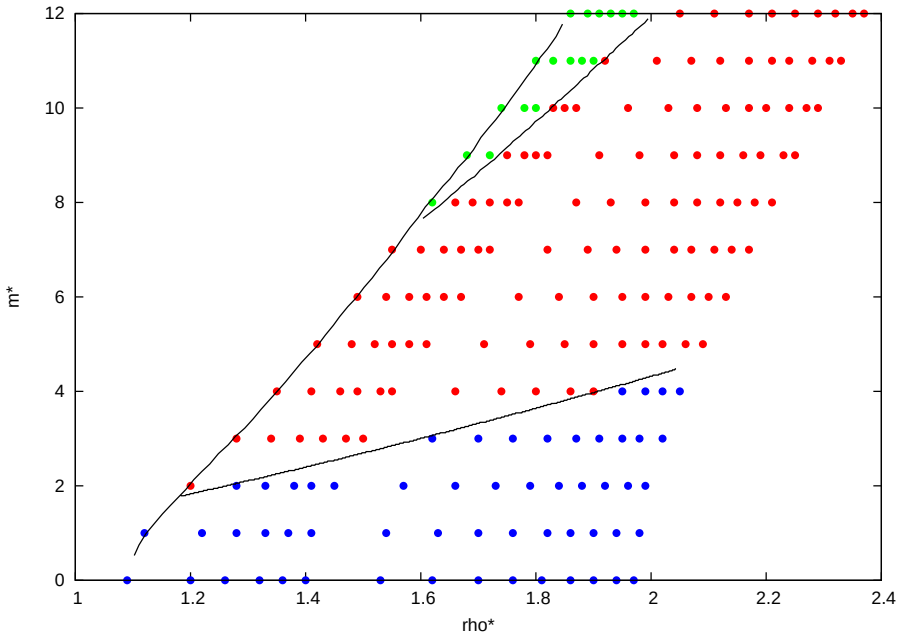

Figure 5.2.: Identified ordered structures for the Stockmayer system in the (m^*, ρ^*)-plane. Symbols: red-bco, green-bct and blue-hexc. The lines are taken from the corresponding phase diagram presented by B. Groh and S. Dietrich [2]. The empty domain at the left is a two-phase region where an infinitely diluted gas coexists with the solid: if a sytem is prepared with a density and a dipole value in this domain, the solid spontaneously shrinks to a smaller volume (the solid has then a higher density), leaving a portion of empty space [2].

hcp, which has an energy very slightly below the fcc value (relative energy difference of the order of $10^{-5} - 10^{-6}$).

We can conclude with B. Groh and S. Dietrich that "at $T = 0$ the Stockmayer crystal in the commonly studied range $m^* \leq 3$ is either hexc or bco, and not fcc nor bct as assumed in various studies before"[2]. For m^* becoming larger, the bct structure can be formed.

6. Summary

In this work we adapted the Ewald summation method to the Stockmayer potential case and implemented it in a phenotype algorithm in order to find the phase diagram of the ground state of a system of dipolar particles. The phenotype algorithm demonstrated once more its power by reaching very often the good structure in a few runs. This enabled us to construct the phase diagram of the studied system with all the dipoles being parallel. We found as in [2] three phases : hexagonal, bco and bct.

Possible improvements of the phenotype algorithm are a population control procedure adapted to the case of dipolar systems and the parallelization of the relaxation procedure, which is the computationnaly most expensive part of the algorithm. The local optimizations of the different individuals are independant, therefore these operations can be parallelized. The computation of the Ewald sums via the FFT transform could also be implemented in order to speed up the calculation.

The phenotype algorithm could also be used to find the phase diagram of the same system of particles but with the orientations of their dipole being able to vary instead of being all fixed in the same direction. Structures with helically varying polarization direction for example, as appeared in simulations of dipolar hard spheres [70], could maybe be found.

Appendices

A. Formalism

According to Bravais [17], a crystalline structure can be represented by its lattice vectors **a**, **b** and **c** (see fig.A.1) and by the coordinates of the particles in the basis cell and the orientation of their dipole.

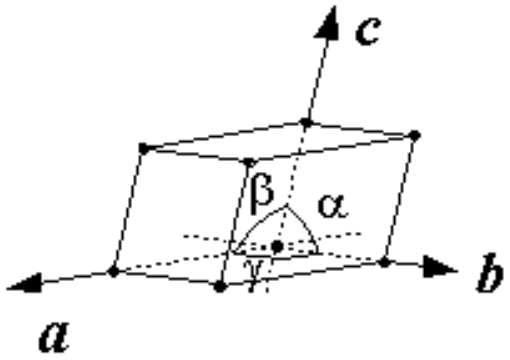

Figure A.1.: Schematic representation of a Bravais lattice

The Cartesian coordinates of the basis vectors are given by

$$\mathbf{a}\begin{pmatrix} a_x \\ a_y \\ a_z \end{pmatrix}_{(x,y,z)}, \ \mathbf{b}\begin{pmatrix} b_x \\ b_y \\ b_z \end{pmatrix}_{(x,y,z)}, \ \mathbf{c}\begin{pmatrix} c_x \\ c_y \\ c_z \end{pmatrix}_{(x,y,z)}, \tag{A.1}$$

the index (x, y, z) meaning that the given coordinates are the Cartesian coordinates.

The volume of the basis cell is given by

$$V_c = \mathbf{a} \cdot (\mathbf{b} \times \mathbf{c}) \tag{A.2}$$

$$= a_x(b_y c_z - b_z c_y) + a_y(b_z c_x - b_x c_z) + a_z(b_x c_y - b_y c_x). \tag{A.3}$$

A.1. Vectors of the real space

In the whole work, i and j refer to particles in the basis cell. In the Ewald sums, the interaction of the particles of the basis with particles of periodic replicas of the basis cell are taken into account. The vector between a particle i of the basis cell and the periodic replica of a particle j of the basis cell is

$$\mathbf{r} = \mathbf{R} + \mathbf{r}_{ij} \tag{A.4}$$

with

$$\mathbf{R} = n_a \cdot \mathbf{a} + n_b \cdot \mathbf{b} + n_c \cdot \mathbf{c} \tag{A.5}$$

where $(n_a, n_b, n_c) \in \mathbb{Z}^3$. The parameter R_{max} of the Ewald sums is in reality $R_{max} = \max(|n_a|, |n_b|, |n_c|) \in \mathbb{N}$ if the cut-off in R space is the same in all three direction, or ($R_{max,a} = \max(|n_a|)$, $R_{max,b} = \max(|n_b|)$, $R_{max,c} = \max(|n_c|)$) if this is not the case. The maximal value of $\|R\|$ in the direction of $\mathbf{a}$ will be in the first case $R_{max} \cdot \|\mathbf{a}\|$, and in the second case $R_{max,a} \cdot \|\mathbf{a}\|$, where $\|\mathbf{a}\|$ is the norm of $\mathbf{a}$.

The Cartesian coordinates of $\mathbf{R}$ are

$$\mathbf{R} \begin{pmatrix} n_a a_x + n_b b_x + n_c c_x \\ n_a a_y + n_b b_y + n_c c_y \\ n_a a_z + n_b b_z + n_c c_z \end{pmatrix}_{(x,y,z)} . \tag{A.6}$$

We furthermore define $R_a = n_a \cdot \|a\|$, $R_b = n_b \cdot \|b\|$ and $R_c = n_c \cdot \|c\|$.

$\mathbf{r}_{ij}$ can be decomposed via the basis vectors as follows

$$\mathbf{r}_{ij} = x_f \cdot \mathbf{a} + y_f \cdot \mathbf{b} + z_f \cdot \mathbf{c}. \tag{A.7}$$

$(x_f, y_f, z_f) \in [0, 1]^3$ are called the *fractional coordinates* of $\mathbf{r}_{ij}$. The Cartesian coordinates of $\mathbf{r}_{ij}$ are then

$$\mathbf{r}_{ij} \begin{pmatrix} x = x_f \cdot a_x + y_f \cdot b_x + z_f \cdot c_x \\ y = x_f \cdot a_y + y_f \cdot b_y + z_f \cdot c_y \\ z = x_f \cdot a_z + y_f \cdot b_z + z_f \cdot c_z \end{pmatrix}_{(x,y,z)} \tag{A.8}$$

We use the following notation: $R = \|\mathbf{R}\|$, $r_{ij} = \|\mathbf{r}_{ij}\|$ and $r = \|\mathbf{r}\|$.

A.2. Wavevectors

A general lattice-vector of the reciprocal lattice is given as a linear combination of the reciprocal basis lattice vectors $\frac{2\pi}{V_c}\mathbf{b}\times\mathbf{c}$, $\frac{2\pi}{V_c}\mathbf{c}\times\mathbf{a}$ and $\frac{2\pi}{V_c}\mathbf{a}\times\mathbf{b}$. We have then

$$\mathbf{k} = \frac{2\pi m}{V_c}\mathbf{b}\times\mathbf{c} + \frac{2\pi n}{V_c}\mathbf{c}\times\mathbf{a} + \frac{2\pi p}{V_c}\mathbf{a}\times\mathbf{b} \tag{A.9}$$

with $(m,n,p)\in\mathbb{Z}^3$, that we write

$$\mathbf{k} = \mathbf{k_a} + \mathbf{k_b} + \mathbf{k_c} \tag{A.10}$$

with

$$\begin{cases} \mathbf{k_a} = \frac{2\pi m}{V_c}\mathbf{b}\times\mathbf{c} \\ \mathbf{k_b} = \frac{2\pi n}{V_c}\mathbf{c}\times\mathbf{a} \\ \mathbf{k_c} = \frac{2\pi p}{V_c}\mathbf{a}\times\mathbf{b} \end{cases} . \tag{A.11}$$

The parameter k_{max} of the Ewald sums is in reality $k_{max} = \max(|m|,|n|,|p|)\in\mathbb{N}$ if the cut-off in k space is the same in all three directions, or $(k_{max,a} = \max(|m|),\ k_{max,b} = \max(|n|),\ k_{max,c} = \max(|p|))$ if this is not the case.

One define

$$k_a = \frac{2\pi}{V_c}m,\ k_b = \frac{2\pi}{V_c}n,\ k_c = \frac{2\pi}{V_c}p. \tag{A.12}$$

Note that $k_a \neq \|\mathbf{k}_a\|$.

The Cartesian coordinates of $\mathbf{k}_a$ are

$$\mathbf{k}_a \begin{pmatrix} k_b(b_yc_z - c_yb_z) \\ k_c(b_zc_x - b_xc_z) \\ k_a(b_xc_y - b_yc_x) \end{pmatrix}_{(x,y,z)} \tag{A.13}$$

and then those of $\mathbf{k}$ are

$$\mathbf{k} \begin{pmatrix} k_x = k_a(b_yc_z - c_yb_z) + k_b(c_ya_z - a_yc_z) + k_c(a_yb_z - b_ya_z) \\ k_y = k_a(b_zc_x - b_xc_z) + k_b(c_za_x - c_xa_z) + k_c(a_zb_x - a_xb_z) \\ k_z = k_a(b_xc_y - b_yc_x) + k_b(c_xa_y - c_ya_x) + k_c(a_xb_y - a_yb_x) \end{pmatrix}_{(x,y,z)} . \tag{A.14}$$

We use the following notation: $k = \|\mathbf{k}\|$.

A.3. Dipole

The absolute value of the dipole $\|\boldsymbol{\mu}\|$ is fixed and is the same for all the particles. Its orientation is given by the spherical coordinates (see fig.A.2) (θ, ψ) and so its Cartesian coordinates are:

$$\boldsymbol{\mu} \begin{pmatrix} \|\boldsymbol{\mu}\| \sin\psi \cos\theta \\ \|\boldsymbol{\mu}\| \sin\psi \sin\theta \\ \|\boldsymbol{\mu}\| \cos\psi \end{pmatrix}_{(x,y,z)} . \tag{A.15}$$

We define $\mu = \|\boldsymbol{\mu}\|$.

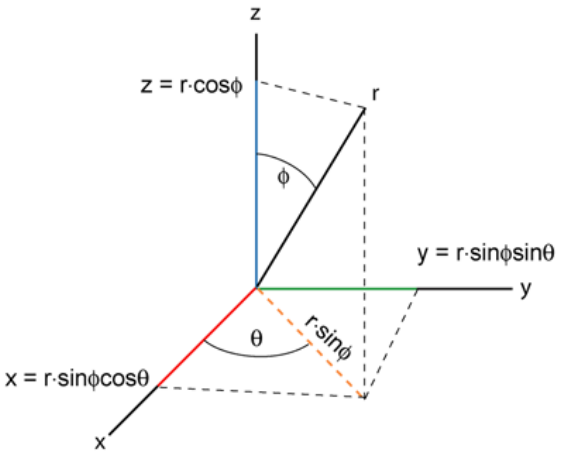

Figure A.2.: Sperical coordinates of a vector [71]

B. Ewald summation formulas for the Gibbs free energy of the system and its derivatives

B.1. Energy

The quantity which has to be minimized in our investigation in order to obtain the ordered stucture of minimum energy is the Gibbs free energy G:

$$G = U + PV - TS \tag{B.1}$$

with

- U the internal energy of the system;
- V its volume;
- S its entropy.

Throughout, the temperature T is considered to be equal to zero, so G is reduced to $G = U + PV$.

For Stockmayer systems, the internal energy can be decomposed as follows:

$$U = U_D + U_{LJ} \tag{B.2}$$

with

$$U_{LJ} = U_{SS}^{(12)} - U_{SS}^{(6)} \tag{B.3}$$

where

- U_D is the dipolar energy;

- U_{LJ} is the Lennard-Jones energy;
- $U_{SS}^{(n)}$ is the internal energy of a the soft sphere system of index n, whose pair potential is given by $V_{SS,pair}^{(n)}(r) = 4\epsilon\left(\frac{\sigma}{r}\right)^n$.

Additional factors, such as $4\pi\epsilon_0$, are omitted for simplicity of notation. All the energies presented in the following are energies of the basis cell.

B.1.1. Dipolar energy

Ewald sum of the dipolar energy

The dipolar energy of a crystal basis cell of N particles, when the relative permittivity of the outside medium ϵ_s is equal to $+\infty$ (metallic boundary condition), is given by [15]

$$\begin{aligned} U_D(\epsilon_s = +\infty) = \frac{1}{2}\sum_{i=1}^{N}\sum_{j=1}^{N}\Bigg(\sum_{\mathbf{R}}{}'(\boldsymbol{\mu}_\mathrm{i}\cdot\boldsymbol{\mu}_\mathrm{j})\mathrm{B}(\mathrm{r},\nu) - (\boldsymbol{\mu}_\mathrm{i}\cdot(\mathbf{R}+\mathbf{r}_\mathrm{ij}))(\boldsymbol{\mu}_\mathrm{j}\cdot(\mathbf{R}+\mathbf{r}_\mathrm{ij}))\mathrm{C}(\mathrm{r},\nu) \\ + \sum_{\mathbf{k}\neq 0}\frac{1}{\pi V_c}(\boldsymbol{\mu}_i\cdot\mathbf{k})(\boldsymbol{\mu}_j\cdot\mathbf{k})(4\pi^2/k^2)\exp(-k^2/4\nu^2)\cos(\mathbf{k}\cdot\mathbf{r}_{ij})\Bigg) \\ - \sum_{i=1}^{N} 2\nu^3\mu_i^2/3\pi^{1/2}. \end{aligned} \tag{B.4}$$

with

$$B(r,\nu) = \frac{\mathrm{erfc}\,(\nu r)}{r^3} + \frac{2\nu}{\sqrt{\pi}}\frac{e^{-\nu^2 r^2}}{r^2}, \tag{B.5}$$

$$C(r,\nu) = -\frac{1}{r}\frac{\partial B}{\partial r} = 3\frac{\mathrm{erfc}\,(\nu r)}{r^3} + \frac{2\nu}{\sqrt{\pi}}(2\nu^2 + \frac{3}{r^2})\frac{e^{-\nu^2 r^2}}{r^2}, \tag{B.6}$$

and $\mathbf{r} = \mathbf{R} + \mathbf{r}_{ij}$ (see A.1). We define

- $$U_{DR} = \frac{1}{2}\sum_{i=1}^{N}\sum_{j=1}^{N}\sum_{\mathbf{R}}{}'\Bigg((\boldsymbol{\mu}_\mathrm{i}\cdot\boldsymbol{\mu}_\mathrm{j})\mathrm{B}(\mathrm{r},\nu) - (\boldsymbol{\mu}_\mathrm{i}\cdot(\mathbf{R}+\mathbf{r}_\mathrm{ij}))(\boldsymbol{\mu}_\mathrm{j}\cdot(\mathbf{R}+\mathbf{r}_\mathrm{ij}))\mathrm{C}(\mathrm{r},\nu)\Bigg); \tag{B.7}$$

- $$U_{DF} = \frac{1}{2}\frac{1}{\pi V_c}\sum_{i=1}^{N}\sum_{j=1}^{N}\sum_{\mathbf{k}\neq 0}\left((\boldsymbol{\mu}_i\cdot\mathbf{k})(\boldsymbol{\mu}_j\cdot\mathbf{k})(4\pi^2/k^2)\exp(-k^2/4\nu^2)\cos(\mathbf{k}\cdot\mathbf{r}_{ij})\right); \tag{B.8}$$

- $$U_{DS} = -\sum_{i=1}^{N} 2\nu^3\mu_i^2/3\pi^{1/2}. \tag{B.9}$$

$U_D(\epsilon_s = +\infty)$ (eq.B.4) is a sum of three terms. The first of these three terms (first line) is the contribution of the real space, it is called U_{DR}. The second term, on the second line, is the contribution of the reciprocal or Fourier space, it is called U_{DF}. It is important to note that the reciprocal space sum includes the interaction of each particle with itself, so a self-energy correction term is needed, which is the so called "self term" U_{DS}: it is the third term (third line). Note also that the interaction of each particle with its own periodic replicas should not be subtracted [72].

If $\epsilon_s = 1$ (vacuum), the energy U_D includes an additionnal term [22], the long range term

$$U_{DLR} = +\frac{1}{2}\sum_{i=1}^{N}\sum_{j=1}^{N}(4\pi/3V_c)\boldsymbol{\mu}_i\cdot\boldsymbol{\mu}_j. \tag{B.10}$$

For other ϵ_s-values, $\epsilon_s \in [1;+\infty]$, one obtains [22]

$$U_D(\epsilon_s) = U_D(\epsilon_s = 1) - \frac{3k_BT}{N\mu^2}y\frac{(\epsilon_s-1)}{(2\epsilon_s+1)}\sum_{i=1}^{N}\sum_{j=1}^{N}\boldsymbol{\mu}_i\cdot\boldsymbol{\mu}_j \tag{B.11}$$

$$= U_D(\epsilon_s = +\infty) + \frac{1}{2}\sum_{i=1}^{N}\sum_{j=1}^{N}(4\pi/3V_c)\boldsymbol{\mu}_i\cdot\boldsymbol{\mu}_j - \frac{3k_BT}{N\mu^2}y\frac{(\epsilon_s-1)}{(2\epsilon_s+1)}\sum_{i=1}^{N}\sum_{j=1}^{N}\boldsymbol{\mu}_i\cdot\boldsymbol{\mu}_j \tag{B.12}$$

with

$$y = \frac{4\pi\rho\mu^2}{9k_BT} \tag{B.13}$$

where ρ is the particle density in the system.

To sum up :

$$U_D = U_{DR} + U_{DF} + U_{DS} + U_{DLR}, \tag{B.14}$$

with $U_{DLR} = 0$ for metallic boundary condition.

Long range term

If the system is surrounded by vacuum ($\epsilon_s = 1$), any polarization of the system will generate surface charges at the interface between the system and the vacuum and these charges, in turn, generate the average (or depolarization) field. A "surface" term or "long range" term U_{DLR} has to be added to U_D. This term vanishes for the choice $\epsilon_s = +\infty$ ("conducting" or "tin-foil" boudary conditions), reflecting the fact that a conducting environment prevents the formation of surface charges and thus suppresses a depolarizing field inside the central cell [15]. For ionic and dipolar systems, where long-range interactions are important, Ewald summation with tinfoil boundary conditions corresponds to the physically most desirable situation [18]. We will thus adopt these conditions and set $U_{DLR} = 0$.

Factorization

The second term of eq. (B.4), U_{DF}, can be factorized, which accelerate the computation :

$$\begin{aligned} U_{DF} =& \frac{1}{2}\sum_{i=1}^{N}\sum_{j=1}^{N}\left(\sum_{\mathbf{k}\neq 0}(1/\pi V_c)(\boldsymbol{\mu}_i\cdot\mathbf{k})(\boldsymbol{\mu}_j\cdot\mathbf{k})(4\pi^2/k^2)\exp(-k^2/4\nu^2)\cos(\mathbf{k}\cdot\mathbf{r}_{ij})\right) \\ =& \frac{2\pi}{V_c}\sum_{\mathbf{k}\neq 0}\frac{1}{k^2}\exp(-k^2/4\nu^2)\tilde{M}(\mathbf{k})\tilde{M}^*(\mathbf{k}) \end{aligned} \tag{B.15}$$

with

$$M(\mathbf{k}) = \sum_{i=1}^{N}(\boldsymbol{\mu}_i\cdot\mathbf{k})\exp(-i\mathbf{k}\cdot\mathbf{r}_i) \tag{B.16}$$

$$= [(\boldsymbol{\mu}_i\cdot\mathbf{k})\cos(\mathbf{k}\cdot\mathbf{r}_i) - i(\boldsymbol{\mu}_i\cdot\mathbf{k})\sin(\mathbf{k}\cdot\mathbf{r}_i)] \tag{B.17}$$

$$\equiv \Re(\tilde{M}(\mathbf{k})) - i\Im(\tilde{M}(\mathbf{k})) \tag{B.18}$$

B.1.2. Lennard-Jones energy

To compute the Ewald sum of the Lennard-Jones energy of the unit cell, the Ewald formula of the sum $\sum_{\mathbf{r}\neq 0} \frac{1}{r^n}$ is needed [2]:

$$\begin{aligned}\sum_{\mathbf{r}\neq 0} \frac{1}{r^n} = \frac{1}{\Gamma(n/2)} \Bigg[& \sum_{\mathbf{r}\neq 0} \frac{1}{r^n} \Gamma(n/2, \nu^2 r^2) \\ & + \frac{\pi^{\frac{3}{2}}}{V_c} \sum_{\mathbf{k}\neq 0} \left(\frac{k}{2}\right)^{n-3} \Gamma\left(\frac{3-n}{2}, \frac{k^2}{4\nu^2}\right) \\ & - \frac{2}{n}\nu^n + N\frac{2}{n-3}\frac{\pi^{\frac{3}{2}}}{V_c}\nu^{n-3} \Bigg]\end{aligned} \tag{B.19}$$

with

- ν a parameter related to the width of the Gaussian distribution;
- $\Gamma(x)$ the Gamma function and $\Gamma(a, x)$ the incomplete Gamma function.

The internal energy of a crystal basis cell of N particles interacting via Lennard-Jones potential is then given by

$$U_{\mathrm{LJ}} = U_{\mathrm{SS}}^{(12)} - U_{\mathrm{SS}}^{(6)} \tag{B.20}$$

where

$$\begin{aligned}U_{\mathrm{SS}}^{(n)} = \frac{2\epsilon\sigma^n}{\Gamma(n/2)} \sum_{i=1}^{N} \Bigg[& \sum_{j=1}^{N} {\sum_{\mathbf{R}}}' \frac{\Gamma(\mathrm{n}/2, \nu^2(\mathbf{R}+\mathbf{r}_{\mathrm{ij}})^2)}{\|\mathbf{R}+\mathbf{r}_{\mathrm{ij}}\|^{\mathrm{n}}} \\ & + \frac{\pi^{\frac{3}{2}}}{V_c} \sum_{\mathbf{k}\neq 0} \sum_{j=1}^{N} \cos(\mathbf{k}\cdot\mathbf{r}_{ij}) \left(\frac{k}{2}\right)^{n-3} \Gamma\left(\frac{3-n}{2}, \frac{k^2}{4\nu^2}\right) \\ & - \frac{2}{n}\nu^n + N\frac{2}{n-3}\frac{\pi^{\frac{3}{2}}}{V_c}\nu^{n-3} \Bigg]\end{aligned} \tag{B.21}$$

with

- ϵ the energy-value at the minimum in the Lennard-Jones potential;
- σ the diameter of the particles (length), i.e. the value of r at which $V_{\mathrm{LJ,\ pair}}(r)$ vanishes;
- the prime indicating that the $i = j$ term must be omitted for $R = 0$ to avoid to take into account the interaction of the particles with itself.

We note that (B.21) can be written as

$$U_{\mathrm{SS}}^{(n)} = U_{\mathrm{SSR}}^{(n)} + U_{\mathrm{SSF}}^{(n)} + U_{\mathrm{SS,\,term3}}^{(n)} + U_{\mathrm{SS,\,term4}}^{(n)} \tag{B.22}$$

with

- $$U_{\mathrm{SSR}}^{(n)} = \frac{2\epsilon\sigma^n}{\Gamma(n/2)} \sum_{i=1}^{N} \sum_{j=1}^{N} {\sum_{\mathbf{R}}}' \frac{\Gamma(\mathrm{n}/2, \nu^2(\mathbf{R}+\mathbf{r}_{\mathrm{ij}})^2)}{\|\mathbf{R}+\mathbf{r}_{\mathrm{ij}}\|^{\mathrm{n}}}; \tag{B.23}$$

- $$U_{\mathrm{SSF}}^{(n)} = \frac{2\epsilon\sigma^n}{\Gamma(n/2)} \frac{\pi^{\frac{3}{2}}}{V_c} \sum_{i=1}^{N} \sum_{\mathbf{k}\neq 0} \sum_{j=1}^{N} \left[\cos(\mathbf{k}\cdot\mathbf{r}_{ij}) \left(\frac{k}{2}\right)^{n-3} \Gamma\left(\frac{3-n}{2}, \frac{k^2}{4\nu^2}\right) \right]; \tag{B.24}$$

- $$U_{\mathrm{SS,\,term3}}^{(n)} = -\frac{2\epsilon\sigma^n}{\Gamma(n/2)} \sum_{i=1}^{N} \left[\frac{2}{n} \nu^n \right]; \tag{B.25}$$

- $$U_{\mathrm{SS,\,term4}}^{(n)} = \frac{2\epsilon\sigma^n}{\Gamma(n/2)} \sum_{i=1}^{N} \left[N \frac{2}{n-3} \frac{\pi^{\frac{3}{2}}}{V_c} \nu^{n-3} \right]. \tag{B.26}$$

B.2. Derivatives of the energy

The forces acting on a particle are given as the sum over the forces originating from the two-particle interactions. The x-component of the force on a particle i originating from its interaction with the particle j can be written as

$$F_{x,i,j} = -\frac{\partial V_{\mathrm{pair(i,j)}}}{\partial x}. \tag{B.27}$$

The total x-component of the force acting on the particle i is then

$$F_{x,i} = -\sum_{j\neq i} \frac{\partial V_{\mathrm{pair(i,j)}}}{\partial x}. \tag{B.28}$$

For the relaxation step in the phenotype algorithm, the gradient of the energy with respect to the parameters to be optimized is needed. It is proportional to the opposite of the forces, we will so calculate the "forces" acting on the system in the same way

as above, also for the components which are not the Cartesian coordinates : the fractional coordinates of the particles, the Cartesian coordinates of the lattice vector and the angles ψ and θ of the dipole orientation.

We will calculate separately the forces originating from the dipolar interaction and from the Lennard-Jones interaction; the forces from the Stockmayer interaction are then the sum of the two contributions.

B.2.1. Derivatives of the dipolar energy

Cartesian and fractional coordinates of the particles

The forces acting on the particle i due to the dipolar interaction are

$$\mathbf{F}_{D,i} = \mathbf{F}_{DR,i} + \mathbf{F}_{DF,i} \tag{B.29}$$

since U_{DLR} and U_{DS} turn out to be independent of the particle i and therefore do not contribute to the dipolar force.

For the contribution of the real space we have

$$\begin{aligned}\mathbf{F}_{DR,i} = &\sum_{j=1}^{N}\sum_{\mathbf{R}}{}'\{[(\boldsymbol{\mu}_{\mathrm{i}}\cdot\boldsymbol{\mu}_{\mathrm{j}})\mathbf{r} + \boldsymbol{\mu}_{\mathrm{i}}(\boldsymbol{\mu}_{\mathrm{j}}\cdot\mathbf{r}) + \boldsymbol{\mu}_{\mathrm{j}}(\boldsymbol{\mu}_{\mathrm{i}}\cdot\mathbf{r})]\mathrm{C}(\mathrm{r},\nu) \\ &- (\boldsymbol{\mu}_i\cdot\mathbf{r})(\boldsymbol{\mu}_j\cdot\mathbf{r})\mathbf{r}D(r,\nu)\}\end{aligned} \tag{B.30}$$

with $C(r,\nu)$ given in (B.6) and

$$\begin{aligned}D(r,\nu) &= -\frac{1}{r}\frac{\partial C}{\partial r} = \frac{1}{r}\frac{\partial}{\partial r}\left(\frac{1}{r}\frac{dB}{dr}\right) \\ &= \frac{1}{r^7}\left[\frac{2\nu r}{\sqrt{\pi}}(15 + 10\nu^2r^2 + 4\nu^4r^4)\exp(-\nu^2r^2) + 15\,\mathrm{erfc}(\nu r)\right]\end{aligned} \tag{B.31}$$

and for the contribution of the reciprocal space:

$$\mathbf{F}_{DF,i} = \frac{4\pi}{V}\sum_{\mathbf{k}\neq 0}\frac{1}{k^2}\exp(-\frac{k^2}{4\nu^2})\sum_{j=1}^{N}\mathbf{k}(\boldsymbol{\mu}_i\cdot\mathbf{k})(\boldsymbol{\mu}_j\cdot\mathbf{k})\sin(\mathbf{k}\cdot\mathbf{r}_{ij}) \tag{B.32}$$

that we can factorize in

$$\begin{aligned}\mathbf{F}_{DF,i} = &\frac{4\pi}{V}\sum_{\mathbf{k}\neq 0}\frac{1}{k^2}\exp(-\frac{k^2}{4\nu^2})\big[\sin(\mathbf{k}\cdot\mathbf{r}_i)\Re(\tilde{M}(\mathbf{k})) \\ &- \cos(\mathbf{k}\cdot\mathbf{r}_i)\Im(\tilde{M}(\mathbf{k}))\big](\boldsymbol{\mu}_i\cdot\mathbf{k})\mathbf{k}.\end{aligned} \tag{B.33}$$

Taking the Cartesian components of the real space contribution to the forces:

$$F_{DR,x,i} = \sum_{j=1}^{N} \sum_{\mathbf{R}}{}' \{[(\boldsymbol{\mu}_{\mathrm{i}} \cdot \boldsymbol{\mu}_{\mathrm{j}})\mathrm{r_x} + \mu_{\mathrm{ix}}(\boldsymbol{\mu}_{\mathrm{j}} \cdot \mathbf{r}) + \mu_{\mathrm{jx}}(\boldsymbol{\mu}_{\mathrm{i}} \cdot \mathbf{r})]\mathrm{C(r,}\nu) - (\boldsymbol{\mu}_i \cdot \mathbf{r})(\boldsymbol{\mu}_j \cdot \mathbf{r}) r_x D(r,\nu)\} \tag{B.34}$$

$$F_{DR,y,i} = \sum_{j=1}^{N} \sum_{\mathbf{R}}{}' \{[(\boldsymbol{\mu}_{\mathrm{i}} \cdot \boldsymbol{\mu}_{\mathrm{j}})\mathrm{r_y} + \mu_{\mathrm{iy}}(\boldsymbol{\mu}_{\mathrm{j}} \cdot \mathbf{r}) + \mu_{\mathrm{jy}}(\boldsymbol{\mu}_{\mathrm{i}} \cdot \mathbf{r})]\mathrm{C(r,}\nu) - (\boldsymbol{\mu}_i \cdot \mathbf{r})(\boldsymbol{\mu}_j \cdot \mathbf{r}) r_y D(r,\nu)\} \tag{B.35}$$

$$F_{DR,z,i} = \sum_{j=1}^{N} \sum_{\mathbf{R}}{}' \{[(\boldsymbol{\mu}_{\mathrm{i}} \cdot \boldsymbol{\mu}_{\mathrm{j}})\mathrm{r_z} + \mu_{\mathrm{iz}}(\boldsymbol{\mu}_{\mathrm{j}} \cdot \mathbf{r}) + \mu_{\mathrm{jz}}(\boldsymbol{\mu}_{\mathrm{i}} \cdot \mathbf{r})]\mathrm{C(r,}\nu) - (\boldsymbol{\mu}_i \cdot \mathbf{r})(\boldsymbol{\mu}_j \cdot \mathbf{r}) r_z D(r,\nu)\}. \tag{B.36}$$

For the reciprocal space contribution, one obtains

$$F_{DF,x,i} = \frac{4\pi}{V} \sum_{\mathbf{k}\neq 0} \frac{1}{k^2} \exp(-\frac{k^2}{4\nu^2}) \sum_{j=1}^{N} k_x (\boldsymbol{\mu}_i \cdot \mathbf{k})(\boldsymbol{\mu}_j \cdot \mathbf{k}) \sin(\mathbf{k} \cdot \mathbf{r}_{ij}) \tag{B.37}$$

and the components along the y- and z-axes can be obtained by replacing x by y and z respectively.

For the fractional coordinates, we have (see A.8):

$$\begin{cases} F_{DR,x_f,i} = a_x F_{DR,x,i} + a_y F_{DR,y,i} + a_z F_{DR,z,i} \\ F_{DR,y_f,i} = b_x F_{DR,x,i} + b_y F_{DR,y,i} + b_z F_{DR,z,i} \\ F_{DR,z_f,i} = c_x F_{DR,x,i} + c_y F_{DR,y,i} + c_z F_{DR,z,i} \end{cases} \tag{B.38}$$

so for x_f for example

$$\begin{aligned} F_{DR,x_f,i} = \sum_{j=1}^{N} \sum_{\mathbf{R}}{}' \Big[& a_x \{[(\boldsymbol{\mu}_i \cdot \boldsymbol{\mu}_j) r_x + \mu_{ix}(\boldsymbol{\mu}_j \cdot \mathbf{r}) + \mu_{jx}(\boldsymbol{\mu}_i \cdot \mathbf{r})] C(r,\nu) \\ & - (\boldsymbol{\mu}_i \cdot \mathbf{r})(\boldsymbol{\mu}_j \cdot \mathbf{r}) r_x D(r,\nu)\} \\ & + a_y \{[(\boldsymbol{\mu}_i \cdot \boldsymbol{\mu}_j) r_y + \mu_{iy}(\boldsymbol{\mu}_j \cdot \mathbf{r}) + \mu_{jy}(\boldsymbol{\mu}_i \cdot \mathbf{r})] C(r,\nu) \\ & - (\boldsymbol{\mu}_i \cdot \mathbf{r})(\boldsymbol{\mu}_j \cdot \mathbf{r}) r_y D(r,\nu)\} \\ & + a_z \{[(\boldsymbol{\mu}_i \cdot \boldsymbol{\mu}_j) r_z + \mu_{iz}(\boldsymbol{\mu}_j \cdot \mathbf{r}) + \mu_{jz}(\boldsymbol{\mu}_i \cdot \mathbf{r})] C(r,\nu) \\ & - (\boldsymbol{\mu}_i \cdot \mathbf{r})(\boldsymbol{\mu}_j \cdot \mathbf{r}) r_z D(r,\nu)\} \Big]. \end{aligned} \tag{B.39}$$

In the above expression, x_f has to be replaced by y_f to obtain $F_{DR,y_f,i}$ and by z_f to obtain $F_{DR,z_f,i}$.

Likewise, for the reciprocal space contribution we obtain

$$\begin{cases} F_{DF,x_f,i} = a_x F_{DF,x,i} + a_y F_{DF,y,i} + a_z F_{DF,z,i} \\ F_{DF,y_f,i} = b_x F_{DF,x,i} + b_y F_{DF,y,i} + b_z F_{DF,z,i} \\ F_{DF,z_f,i} = c_x F_{DF,x,i} + c_y F_{DF,y,i} + c_z F_{DF,z,i} \end{cases} ; \tag{B.40}$$

so, for example,

$$F_{DF,x_f,i} = \frac{4\pi}{V} \sum_{\mathbf{k}\neq 0} \frac{1}{k^2} \exp(-\frac{k^2}{4\nu^2}) \sum_{j=1}^{N} \Big[(\boldsymbol{\mu}_i \cdot \mathbf{k})(\boldsymbol{\mu}_j \cdot \mathbf{k}) \sin(\mathbf{k} \cdot \mathbf{r}_{ij})(k_x a_x + k_y a_y + k_z a_z) \Big]. \tag{B.41}$$

a has to be replaced by b to obtain $F_{DF,y_f,i}$ and by c to obtain $F_{DF,z_f,i}$.

Dipole orientation

The dipole and its orientation are only present in the first two terms of the dipolar energy (see eq.(B.4)), therefore

$$F_{D,\theta,i} = F_{DR,\theta,i} + F_{DF,\theta,i} \tag{B.42}$$

and

$$F_{D,\psi,i} = F_{DR,\psi,i} + F_{DF,\psi,i} \tag{B.43}$$

with

$$F_{DR,\theta,i} = \sum_{j=1}^{N} \sum_{\mathbf{R}}{}' \Bigg(\big(\mu_{iy}\mu_{jx} - \mu_{ix}\mu_{jy}\big) B(\mathbf{R} + \mathbf{r}_{ij}, \nu) - \big(\mu_{iy}(\mathbf{R} + \mathbf{r}_{ij})_x - \mu_{ix}(\mathbf{R} + \mathbf{r}_{ij})_y\big)(\mu_j \cdot (\mathbf{R} + \mathbf{r}_{ij}))C(\mathbf{R} + \mathbf{r}_{ij}, \nu) \Bigg), \tag{B.44}$$

$$F_{DR,\psi,i} = -\|\mu\| \sum_{j=1}^{N} \sum_{\mathbf{R}}{}' \Bigg(\big(\cos\theta_{\mathrm{i}} \cos\psi_{\mathrm{i}} \mu_{\mathrm{jx}} + \sin\theta_{\mathrm{i}} \cos\psi_{\mathrm{i}} \mu_{\mathrm{jy}} - \sin\psi_{\mathrm{i}} \mu_{\mathrm{jz}} \big) \mathrm{B}(\mathbf{R} + \mathbf{r}_{\mathrm{ij}}, \nu) - \big(\cos\theta_i \cos\psi_i (\mathbf{R} + \mathbf{r}_{ij})_x + \sin\theta_i \cos\psi_i (\mathbf{R} + \mathbf{r}_{ij})_y - \sin\psi_i (\mathbf{R} + \mathbf{r}_{ij})_z \big) (\boldsymbol{\mu}_j \cdot (\mathbf{R} + \mathbf{r}_{ij})) C(\mathbf{R} + \mathbf{r}_{ij}, \nu) \Bigg), \tag{B.45}$$

$$F_{DF,\theta,i} = \frac{4\pi}{V_c}\sum_{\mathbf{k}\neq 0}\frac{1}{k^2}\exp\left(\frac{-k^2}{4\nu^2}\right)(\mu_{iy}k_x - \mu_{ix}k_y)\Big(\cos(\mathbf{k}\cdot\mathbf{r}_i)\Re(\tilde{M}) + \sin(\mathbf{k}\cdot\mathbf{r}_i)\Im(\tilde{M})\Big), \tag{B.46}$$

$$F_{DF,\psi,i} = -\frac{4\pi}{V_c}\|\mu\|\sum_{\mathbf{k}\neq 0}\Bigg(\frac{1}{k^2}\exp\left(\frac{-k^2}{4\nu^2}\right)\Big(\cos\psi_i\cos\theta_i k_x + \cos\psi_i\sin\theta_i k_y - \sin\psi_i k_z\Big) \Big(\cos(\mathbf{k}\cdot\mathbf{r}_i)\Re(\tilde{M}) + \sin(\mathbf{k}\cdot\mathbf{r}_i)\Im(\tilde{M})\Big)\Bigg). \tag{B.47}$$

Cartesian coordinates of lattice vectors

The lattice parameters are only present in the first two terms of the dipolar energy (see eq.(B.4)) so for example for the derivative with respect to a_x we obtain

$$F_{D,a_x} = F_{DR,a_x} + F_{DF,a_x} \tag{B.48}$$

The forces considered here act on the whole system and not only on a particle, there is therefore an additional sum over i.

- Real space contribution

$$F_{DR,a_x} = -\sum_{i=1}^{N}\sum_{j=1}^{N}\sum_{\mathbf{R}}{}'\left(\frac{\mathrm{R_a}}{\|\mathrm{a}\|} + \mathrm{x_f}\right)\Bigg[r_x\Big(-(\boldsymbol{\mu}_i\cdot\boldsymbol{\mu}_j)C(r,\nu) + (\boldsymbol{\mu}_i\cdot\mathbf{r})(\boldsymbol{\mu}_j\cdot\mathbf{r})D(r,\nu)\Big) - \Big(\boldsymbol{\mu}_{ix}(\boldsymbol{\mu}_j\cdot\mathbf{r}) + (\boldsymbol{\mu}_i\cdot\mathbf{r})\boldsymbol{\mu}_{jx}\Big)C(r,\nu)\Bigg]. \tag{B.49}$$

  x has to be replaced by y to obtain F_{DR,a_y} and by z to obtain F_{DR,a_z}. a has to be replaced by b to obtain F_{DR,b_x}, etc.

- Reciprocal space contribution

$$F_{DF,a_x} = -\frac{4\pi}{V_c}\sum_{\mathbf{k}\neq 0}\frac{\exp\left(-k^2/(4\nu^2)\right)}{k^2}\sum_{i=1}^{N}\sum_{j=1}^{N}\cos(\mathbf{k}\cdot\mathbf{r}_{ij})(\boldsymbol{\mu}_j\cdot\mathbf{k}) \Bigg[-(\boldsymbol{\mu}_i\cdot\mathbf{k})\Big(\frac{1}{V_c}\frac{\partial V_c}{\partial a_x} + \Big(\frac{2}{k} + \frac{k}{2\nu^2}\Big)\frac{\partial k}{\partial a_x}\Big) + 2Bprim_{a_x}\Bigg] \tag{B.50}$$

  that we can factorize in

$$F_{DF,a_x} = -\frac{4\pi}{V_c}\sum_{\mathbf{k}\neq 0}\frac{\exp\left(-k^2/(4\nu^2)\right)}{k^2}\sum_{i=1}^{N}\sum_{j=1}^{N}\Big(\cos(\mathbf{k}\cdot\mathbf{r}_i)\Re(\tilde{M}) + \sin(\mathbf{k}\cdot\mathbf{r}_i)\Im(\tilde{M})\Big) \Bigg[-(\boldsymbol{\mu}_i\cdot\mathbf{k})\Big(\frac{1}{V_c}\frac{\partial V_c}{\partial a_x} + \Big(\frac{2}{k} + \frac{k}{2\nu^2}\Big)\frac{\partial k}{\partial a_x}\Big) + 2Bprim_{a_x}\Bigg]. \tag{B.51}$$

x has to be replaced by y to obtain F_{DF,a_y} and by z to obtain F_{DF,a_z}, a has to be replaced by b to obtain F_{DF,b_x}, using the following expressions

$$
\begin{aligned}
Bprim_{a_x} &= -m_{iy}(-k_b c_z + k_c b_z) + m_{iz}(-k_b c_y + k_c b_y) - (m_{ix}k_x + m_{iy}k_y + m_{iz}k_z)\frac{1}{V_c}\frac{\partial V_c}{\partial a_x};\\
Bprim_{a_y} &= m_{ix}(-k_b c_z + k_c b_z) + m_{iz}(k_b c_x - k_c b_x) - (m_{ix}k_x + m_{iy}k_y + m_{iz}k_z)\frac{1}{V_c}\frac{\partial V_c}{\partial a_y};\\
Bprim_{a_z} &= m_{ix}(k_b c_y - k_c b_y) - m_{iy}(k_b c_x - k_c b_x) - (m_{ix}k_x + m_{iy}k_y + m_{iz}k_z)\frac{1}{V_c}\frac{\partial V_c}{\partial a_z};\\
Bprim_{b_x} &= -m_{iy}(k_a c_z - k_c a_z) + m_{iz}(k_a c_y - k_c a_y) - (m_{ix}k_x + m_{iy}k_y + m_{iz}k_z)\frac{1}{V_c}\frac{\partial V_c}{\partial b_x};\\
Bprim_{b_y} &= m_{ix}(k_a c_z - k_c a_z) + m_{iz}(-k_a c_x + k_c a_x) - (m_{ix}k_x + m_{iy}k_y + m_{iz}k_z)\frac{1}{V_c}\frac{\partial V_c}{\partial b_y};\\
Bprim_{b_z} &= m_{ix}(-k_a c_y + k_c a_y) - m_{iy}(-k_a c_x + k_c a_x) - (m_{ix}k_x + m_{iy}k_y + m_{iz}k_z)\frac{1}{V_c}\frac{\partial V_c}{\partial b_z};\\
Bprim_{c_x} &= -m_{iy}(-k_a b_z + k_b a_z) + m_{iz}(-k_a b_y + k_b a_y) - (m_{ix}k_x + m_{iy}k_y + m_{iz}k_z)\frac{1}{V_c}\frac{\partial V_c}{\partial c_x};\\
Bprim_{c_y} &= m_{ix}(-k_a b_z + k_b a_z) + m_{iz}(k_a b_x - k_b a_x) - (m_{ix}k_x + m_{iy}k_y + m_{iz}k_z)\frac{1}{V_c}\frac{\partial V_c}{\partial c_y};\\
Bprim_{c_z} &= m_{ix}(k_a b_y - k_b a_y) - m_{iy}(k_a b_x - k_b a_x) - (m_{ix}k_x + m_{iy}k_y + m_{iz}k_z)\frac{1}{V_c}\frac{\partial V_c}{\partial c_z}.
\end{aligned}
\tag{B.52}
$$

B.2.2. Derivatives of the Lennard-Jones energy

In the following we will consider the derivatives of the soft sphere energy: to obtain the value of one derivative of the Lennard-Jones energy, it is sufficent to calculate the difference between the corresponding derivatives of the soft sphere energy for $n = 12$ and the corresponding derivative of the soft sphere energy for $n = 6$.

Cartesian and fractional coordinates of the particles

The forces acting on the particle i due to the soft sphere interaction are given by

$$\mathbf{F}_{SSn,i} = \mathbf{F}_{SSnR,i} + \mathbf{F}_{SSnF,i}, \tag{B.53}$$

since $U^{(n)}_{\text{SS, term3}}$ and $U^{(n)}_{\text{SS, term4}}$ turn out to be independent of particle i and therefore do not contribute to the Lennard-Jones force.

For the contribution of the real space we have

$$\mathbf{F}_{SSnR,i} = -\frac{4\epsilon\sigma^n}{\Gamma(n/2)} \sum_{j=1}^{N} \sum_{\mathbf{R}}{}' \Bigg[\Bigg(\frac{2\nu^2 \Gamma'(\frac{n}{2}, \nu^2 \|\mathbf{R} + \mathbf{r}_{ij}\|^2)}{\|\mathbf{R} + \mathbf{r}_{ij}\|^{n-1}} - \frac{\Gamma(\frac{n}{2}, \nu^2 \|\mathbf{R} + \mathbf{r}_{ij}\|^2) n}{\|\mathbf{R} + \mathbf{r}_{ij}\|^{n+1}} \Bigg) \frac{\mathbf{R} + \mathbf{r}_{ij}}{\|\mathbf{R} + \mathbf{r}_{ij}\|} \Bigg] \tag{B.54}$$

with

$$\Gamma'(a, x) = \frac{\partial \Gamma(a, x)}{\partial x} = -x^{a-1} e^{-x}, \tag{B.55}$$

and

$$\mathbf{F}_{SSnF,i} = \frac{4\epsilon\sigma^n}{\Gamma(n/2)} \frac{\pi^{3/2}}{V_c} \sum_{\mathbf{k} \neq 0} \sum_{j=1}^{N} \sin(\mathbf{k} \cdot \mathbf{r}_{ij}) \left(\frac{k}{2} \right)^{n-3} \Gamma\left(\frac{3-n}{2}, \frac{k^2}{4\nu^2} \right) \cdot \mathbf{k}. \tag{B.56}$$

Taking the Cartesian components of the real space contribution to the forces:

$$F_{SSnR,x,i} = -\frac{4\epsilon\sigma^n}{\Gamma(n/2)} \sum_{j=1}^{N} \sum_{\mathbf{R}}{}' \Bigg[\Bigg(\frac{2\nu^2 \Gamma'(\frac{n}{2}, \nu^2 \|\mathbf{R} + \mathbf{r}_{ij}\|^2)}{\|\mathbf{R} + \mathbf{r}_{ij}\|^{n-1}} - \frac{\Gamma(\frac{n}{2}, \nu^2 \|\mathbf{R} + \mathbf{r}_{ij}\|^2) n}{\|\mathbf{R} + \mathbf{r}_{ij}\|^{n+1}} \Bigg) \frac{R_x + r_{ijx}}{\|\mathbf{R} + \mathbf{r}_{ij}\|} \Bigg] \tag{B.57}$$

and the components along y and z can be obtained by replacing x by y and z, respectively.

For the reciprocal space contribution we obtain

$$F_{SSnF,x,i} = \frac{4\epsilon\sigma^n}{\Gamma(n/2)} \frac{\pi^{3/2}}{V_c} \sum_{\mathbf{k} \neq 0} \sum_{j=1}^{N} \sin(\mathbf{k} \cdot \mathbf{r}_{ij}) \left(\frac{k}{2} \right)^{n-3} \Gamma\left(\frac{3-n}{2}, \frac{k^2}{4\nu^2} \right) \cdot k_x \tag{B.58}$$

and the components along y and z can be obtained by replacing x by y and z, respectively.

For the fractional coordinates, we have (see A.8):

$$\begin{cases} F_{SSnR,x_f,i} = a_x F_{SSnR,x,i} + a_y F_{SSnR,y,i} + a_z F_{SSnR,z,i} \\ F_{SSnR,y_f,i} = b_x F_{SSnR,x,i} + b_y F_{SSnR,y,i} + b_z F_{SSnR,z,i} \\ F_{SSnR,z_f,i} = c_x F_{SSnR,x,i} + c_y F_{SSnR,y,i} + c_z F_{SSnR,z,i} \end{cases} \tag{B.59}$$

so for x_f for example

$$F_{SSnR,x_f,i} = -\frac{4\epsilon\sigma^n}{\Gamma(n/2)} \sum_{j=1}^{N} \sum_{\mathbf{R}}{}' \Bigg[\Bigg(\frac{2\nu^2 \Gamma'(\frac{n}{2}, \nu^2 \|\mathbf{R} + \mathbf{r}_{ij}\|^2)}{\|\mathbf{R} + \mathbf{r}_{ij}\|^{n-1}} - \frac{\Gamma(\frac{n}{2}, \nu^2 \|\mathbf{R} + \mathbf{r}_{ij}\|^2) n}{\|\mathbf{R} + \mathbf{r}_{ij}\|^{n+1}} \Bigg) \frac{(R_x + r_{ijx}) a_x + (R_y + r_{ijy}) a_y + (R_z + r_{ijz}) a_z}{\|\mathbf{R} + \mathbf{r}_{ij}\|} \Bigg]. \tag{B.60}$$

a has to be replaced by b to obtain $F_{SSnR,y_f,i}$ and by c to obtain $F_{SSnR,z_f,i}$.

Likewise, for the reciprocal space contribution :

$$\begin{cases} F_{SSnF,x_f,i} = a_x F_{SSnF,x,i} + a_y F_{SSnF,y,i} + a_z F_{SSnF,z,i} \\ F_{SSnF,y_f,i} = b_x F_{SSnF,x,i} + b_y F_{SSnF,y,i} + b_z F_{SSnF,z,i} \\ F_{SSnF,z_f,i} = c_x F_{SSnF,x,i} + c_y F_{SSnF,y,i} + c_z F_{SSnF,z,i} \end{cases} \tag{B.61}$$

and so

$$F_{SSnF,x_f,i} = \frac{4\epsilon\sigma^n}{\Gamma(n/2)} \frac{\pi^{3/2}}{V_c} \sum_{\mathbf{k}\neq 0} \sum_{j=1}^{N} \sin(\mathbf{k}\cdot\mathbf{r}_{ij}) \left(\frac{k}{2}\right)^{n-3} \Gamma\left(\frac{3-n}{2}, \frac{k^2}{4\nu^2}\right) (k_x a_x + k_y a_y + k_z a_z). \tag{B.62}$$

a has to be replaced by b to obtain $F_{SSnF,y_f,i}$ and by c to obtain $F_{SSnF,z_f,i}$.

Cartesian coordinates of lattice vectors

The lattice parameters are present in the first two terms and in the fourth term of the soft sphere energy (see eq.(B.21)) so for example for a_x we obtain

$$F_{SSn,a_x} = F_{SSnR,a_x} + F_{SSnF,a_x} + F_{SSn-term4,a_x} \tag{B.63}$$

The forces considered here act on the whole system and not only on a particle.

- Real space contribution

$$F_{SSnR,a_x} = -\frac{4\epsilon\sigma^n}{\Gamma(n/2)} \sum_{i=1}^{N} \sum_{j=1}^{N} \sum_{\mathbf{R}}{}' \left[\left(\frac{2\nu^2 \Gamma'(\frac{n}{2}, \nu^2 \|\mathbf{R}+\mathbf{r}_{ij}\|^2)}{\|\mathbf{R}+\mathbf{r}_{ij}\|^{n-1}} - \frac{\Gamma(\frac{n}{2}, \nu^2\|\mathbf{R}+\mathbf{r}_{ij}\|^2) n}{\|\mathbf{R}+\mathbf{r}_{ij}\|^{n+1}} \right) \frac{(R_x + r_{ijx}) \cdot Term_a}{\|\mathbf{R}+\mathbf{r}_{ij}\|} \right] \tag{B.64}$$

  with

$$Term_a = n_a + x_f = \frac{R_a}{\|a\|} + x_f \tag{B.65}$$

$$Term_b = n_b + y_f = \frac{R_b}{\|b\|} + y_f \tag{B.66}$$

$$Term_c = n_c + z_f = \frac{R_c}{\|c\|} + z_f. \tag{B.67}$$

  x has to be replaced by y to obtain F_{SSnR,a_y} and by z to obtain F_{SSnR,a_z}. a has to be replaced by b to obtain F_{SSnR,b_x}.

- Reciprocal space contribution

$$F_{SSnF,a_x} = -\frac{4\epsilon\sigma^n}{\Gamma(n/2)}\frac{\pi^{3/2}}{V_c}\sum_{\mathbf{k}\neq 0}\sum_{i=1}^{N}\sum_{j=1}^{N}\cos(\mathbf{k}\cdot\mathbf{r}_{ij})\Bigg[\left(\frac{n-3}{2}\left(\frac{k}{2}\right)^{n-4}\Gamma\left(\frac{3-n}{2},\frac{k^2}{4\nu^2}\right) + \left(\frac{k}{2}\right)^{n-3}\frac{k}{2\nu^2}\Gamma'\left(\frac{3-n}{2},\frac{k^2}{4\nu^2}\right)\right)\frac{\partial k}{\partial a_x} + \left(\frac{k}{2}\right)^{n-3}\Gamma\left(\frac{3-n}{2},\frac{k^2}{4\nu^2}\right)\left(-\frac{\partial V_c}{\partial a_x}\right)\frac{1}{V_c}\Bigg] \tag{B.68}$$

x has to be replaced by y to obtain F_{SSnF,a_y} and by z to obtain F_{SSnF,a_z}. a has to be replaced by b to obtain F_{SSnF,b_x}. V_c is the volume of the unit cell.

In those expressions, the derivatives of k with respect to the lattice parameters are given by

$$\begin{aligned}
\frac{\partial k}{\partial a_x} &= \frac{k_y(k_c b_z - k_b c_z) + k_z(k_c b_y - k_b c_y)}{k} - \frac{k}{V_c}\frac{\partial V_c}{\partial a_x};\\
\frac{\partial k}{\partial a_y} &= \frac{k_x(k_c b_z - k_b c_z) + k_z(k_b c_x - k_c b_x)}{k} - \frac{k}{V_c}\frac{\partial V_c}{\partial a_y};\\
\frac{\partial k}{\partial a_z} &= \frac{k_x(k_b c_y - k_c b_y) + k_y(k_b c_x - k_c b_x)}{k} - \frac{k}{V_c}\frac{\partial V_c}{\partial a_z};\\
\frac{\partial k}{\partial b_x} &= \frac{k_y(k_a c_z - k_c a_z) + k_z(k_a c_y - k_c a_y)}{k} - \frac{k}{V_c}\frac{\partial V_c}{\partial b_x};\\
\frac{\partial k}{\partial b_y} &= \frac{k_x(k_a c_z - k_c a_z) + k_z(k_c a_x - k_a c_x)}{k} - \frac{k}{V_c}\frac{\partial V_c}{\partial b_y};\\
\frac{\partial k}{\partial b_z} &= \frac{k_x(k_c a_y - k_a c_y) + k_y(k_c a_x - k_a c_x)}{k} - \frac{k}{V_c}\frac{\partial V_c}{\partial b_z};\\
\frac{\partial k}{\partial c_x} &= \frac{k_y(k_b a_z - k_a b_z) + k_z(k_b a_y - k_a b_y)}{k} - \frac{k}{V_c}\frac{\partial V_c}{\partial c_x};\\
\frac{\partial k}{\partial c_y} &= \frac{k_x(k_b a_z - k_a b_z) + k_z(k_a b_x - k_b a_x)}{k} - \frac{k}{V_c}\frac{\partial V_c}{\partial c_y};\\
\frac{\partial k}{\partial c_z} &= \frac{k_x(k_a b_y - k_b a_y) + k_y(k_a b_x - k_b a_x)}{k} - \frac{k}{V_c}\frac{\partial V_c}{\partial c_z}
\end{aligned} \tag{B.69}$$

and the derivatives of V_c with respect to the lattice parameters are given by

$$\begin{aligned}
\frac{\partial V_c}{\partial a_x} &= b_y c_z - b_z c_y; \\
\frac{\partial V_c}{\partial a_y} &= b_z c_x - b_x c_z; \\
\frac{\partial V_c}{\partial a_z} &= b_x c_y - b_y c_x; \\
\frac{\partial V_c}{\partial b_x} &= a_z c_y - a_y c_z; \\
\frac{\partial V_c}{\partial b_y} &= a_x c_z - a_z c_x; \\
\frac{\partial V_c}{\partial b_z} &= a_y c_x - a_x c_y; \\
\frac{\partial V_c}{\partial c_x} &= a_y b_z - a_z b_y; \\
\frac{\partial V_c}{\partial c_y} &= a_z b_x - a_x b_z; \\
\frac{\partial V_c}{\partial c_z} &= a_x b_y - a_y b_x.
\end{aligned} \tag{B.70}$$

- Fourth term contribution

$$F_{SSn-term4,a_x} = \sum_{i=0}^{N} \frac{8N\epsilon\sigma^n\pi^{3/2}\nu^{n-3}}{\Gamma(n/2)(n-3)V_c^2}\frac{\partial V_c}{\partial a_x} \tag{B.71}$$

  x has to be replaced by y to obtain $F_{SSn-term4,a_y}$ and by z to obtain $F_{SSn-term4,a_z}$. a has to be replaced by b to obtain $F_{SSn-term4,b_x}$.

B.3. The Gibbs free energy and its derivatives

To obtain the Gibbs free energy of the unit cell of a Stockmayer crystal, we have to add to the internal energy computed with the expressions given in Appendix B.1 a term PV_c. For the forces, the only changement is in the derivative with respect to the lattice coordinates. If we only consider the internal energy, we have

$$F_{\text{Stockmayer},a_x} = F_{SSn,a_x} + F_{SSnF,a_x} + F_{D,a_x} \tag{B.72}$$

but if we consider the Gibbs free energy, we have

$$F_{\text{Stockmayer},a_x} = F_{SSn,a_x} + F_{SSnF,a_x} + F_{D,a_x} - 2P\frac{\partial V_c}{\partial a_x}. \tag{B.73}$$

C. Three-dimensional Bravais lattices and crystal structures

In this appendix we will describe some crystal structures that intervene in this thesis. Lattice structures can be described thanks to the 14 Bravais lattices (see fig. C.1). The lattice centerings are

- P: primitive centering, the lattice points are only on the corners,
- I: body centered, there is one additional point at the center of the cell,
- F: face centered, the lattice points are on the corners of the cell and at the center of each of the faces of the cell,
- A, B or C: centered on a single face, the lattice points are on the corners of the cell and at the center of one of the faces of the cell.

C.1. fcc

The face centered cubic lattice (fcc, see fig.C.2) is a cubic structure belonging to the space group class $Fm\bar{3}m$ (number 225) [68]. It is one of the two most common arrangements of particles in solid state physics and guarantees a close packing of the particles : the structure is thus also called "cubic close packing". The stackering sequence of layers is of the type ABCABC... (see fig. C.3).

The conventional simple unit cell of the fcc structure can be described via its three lattice vectors (primitive vectors) and one basis particle (basis vector):

Primitive Vectors:

$\mathbf{a} = \frac{1}{2}a\hat{\mathbf{e}}_y + \frac{1}{2}a\hat{\mathbf{e}}_z$,

$\mathbf{b} = \frac{1}{2}a\hat{\mathbf{e}}_x + \frac{1}{2}a\hat{\mathbf{e}}_z$,

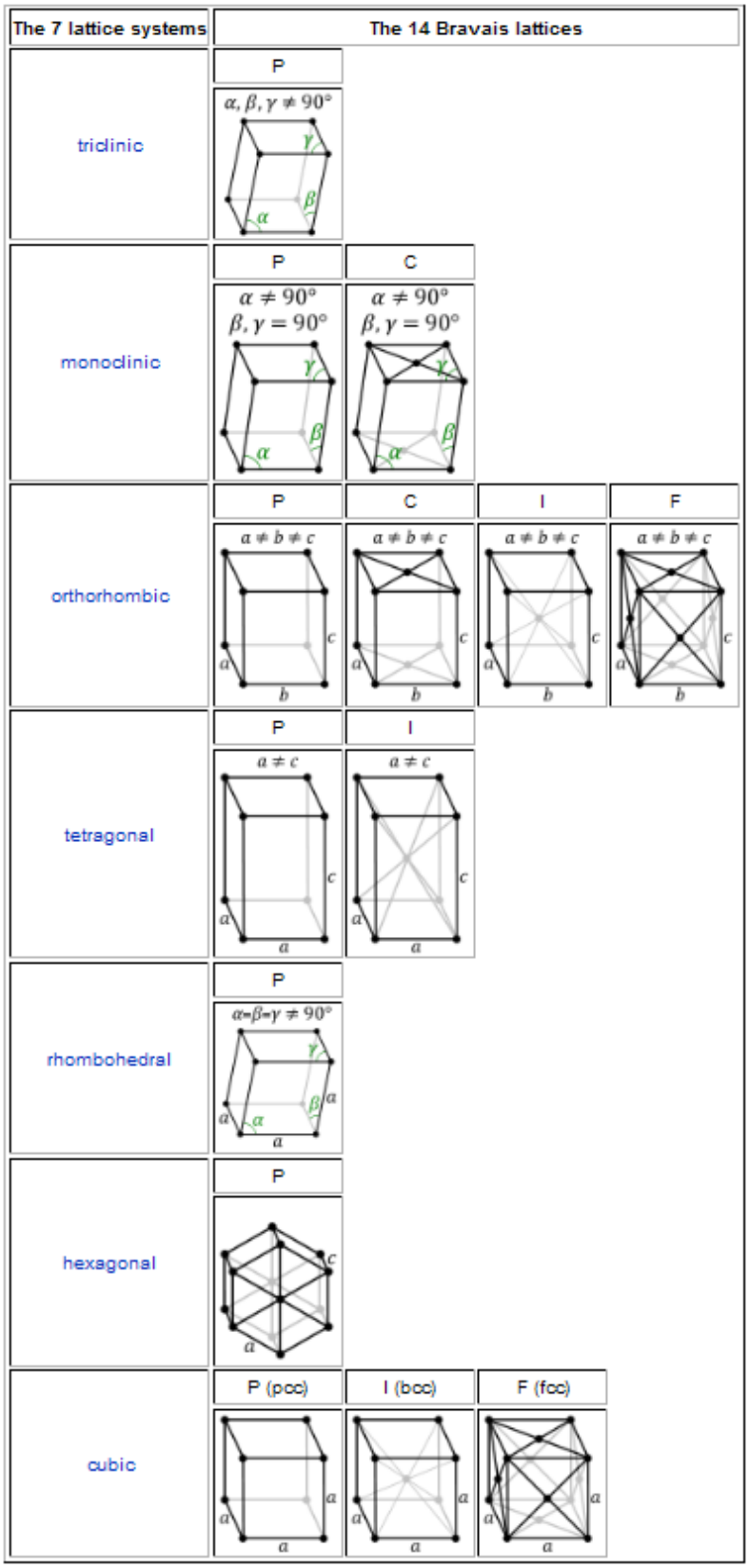

Figure C.1.: Bravais lattices and their lattice systems [73]

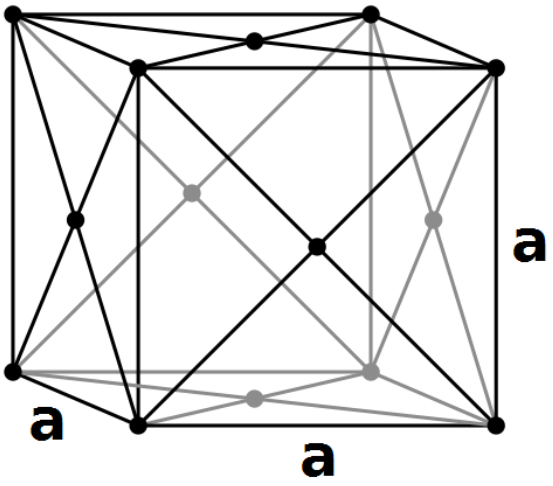

Figure C.2.: Conventional (non-simple) unit cell of the fcc lattice

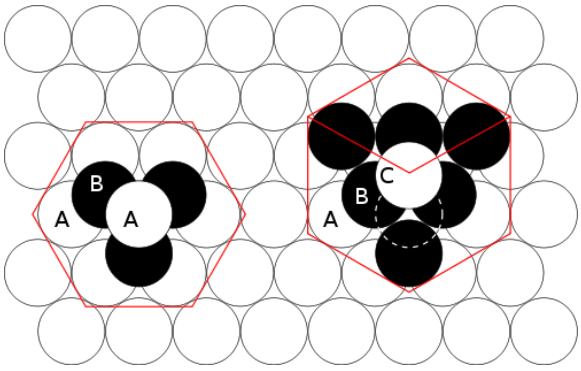

Figure C.3.: Two possibilities of close packing: the hcp lattice (left) and the fcc lattice (right) [74]

$\mathbf{c} = \frac{1}{2}a\hat{\mathbf{e}}_x + \frac{1}{2}a\hat{\mathbf{e}}_y$;

Basis Vector:

$\mathbf{B}_1 = \vec{0}$.

C.2. hcp and hexc

The hexagonal closest-packing lattice (hcp, see fig.C.4) is an hexagonal structure belonging to the space group class $P6_3/mmc$ (number 194) [68]. It is the other of the two most common particle arrangements in solid state physics. The stackering sequence of layers is of the type ABAB... (see fig. C.3).

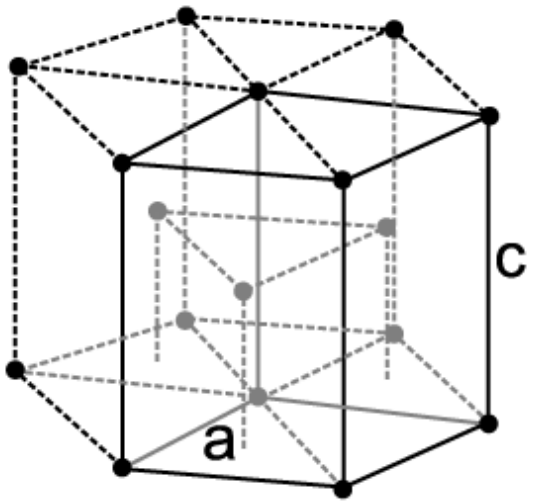

Figure C.4.: Conventional unit cell of the hcp lattice

The conventional unit cell of the hcp lattice can be described via its three lattice vectors (primitive vectors) and two basis particles (basis vectors):

Primitive Vectors:

$\mathbf{a} = \frac{1}{2}a\hat{\mathbf{e}}_x - \frac{1}{2}\sqrt{3}a\hat{\mathbf{e}}_y$,

$\mathbf{b} = \frac{1}{2}a\hat{\mathbf{e}}_x + \frac{1}{2}\sqrt{3}a\hat{\mathbf{e}}_y$,

$\mathbf{c} = c\hat{\mathbf{e}}_z$;

Basis Vector:

$\mathbf{B}_1 = \frac{1}{3}\mathbf{a} + \frac{2}{3}\mathbf{b} + \frac{1}{4}\mathbf{c} = \frac{1}{2}a\hat{\mathbf{e}}_x + \frac{1}{2\sqrt{3}}a\hat{\mathbf{e}}_y + \frac{1}{4}c\hat{\mathbf{e}}_z,$

$\mathbf{B}_2 = \frac{2}{3}\mathbf{a} + \frac{1}{3}\mathbf{b} + \frac{3}{4}\mathbf{c} = \frac{1}{2}a\hat{\mathbf{e}}_x - \frac{1}{2\sqrt{3}}a\hat{\mathbf{e}}_y + \frac{3}{4}c\hat{\mathbf{e}}_z.$

Note that $\frac{c}{a} = \sqrt{\frac{8}{3}}$ for the hcp structure. We will note hexc a structure which is similar to hcp but which can be slightly extended or shrinked along the c-axis, so that $\frac{c}{a}$ can be different from $\sqrt{\frac{8}{3}}$.

C.3. bct

The body-centered tetragonal lattice (bct, see fig.C.5) is a tetragonal lattice belonging to the space group class $I4/mmm$ (number 139) [68]. It is a distortion of the bcc lattice (see fig.C.1).

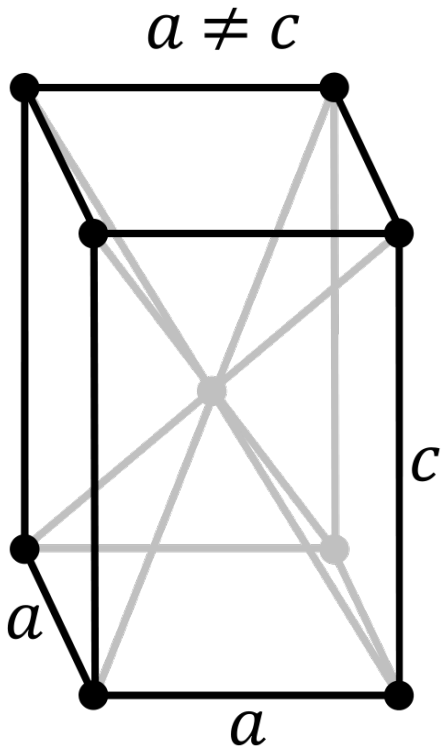

Figure C.5.: Conventional (non-simple) unit cell of the bct lattice

The conventional simple unit cell of the bct lattice can be described via its three lattice vectors (primitive vectors) and one basis particle (basis vector):

Primitive Vectors:

$\mathbf{a} = a\hat{\mathbf{e}}_x$,

$\mathbf{b} = a\hat{\mathbf{e}}_y$,

$\mathbf{c} = \frac{1}{2}a\hat{\mathbf{e}}_x + \frac{1}{2}a\hat{\mathbf{e}}_y + \frac{1}{2}c\hat{\mathbf{e}}_z$;

Basis Vector:

$\mathbf{B}_1 = \vec{0}$.

C.4. bco

The body centered orthorombic lattice (bco, see fig.C.6) is an orthorombic structure belonging to the space group class $Immm$ (number 71) [68]. Orthorhombic lattices result from stretching a cubic lattice along two of its axes by two different factors, resulting in a rectangular prism with a rectangular base (a by b) and height (c), such that a, b and c are distinct. All three bases intersect at 90°angles. The three lattice vectors remain mutually orthogonal. Three lattice vectors (primitive vectors) and one basis particle (basis vector) in (0,0,0) are sufficient to describe the conventional simple unit cell of the bco lattice. This structure reduces to bct for $a = b$.

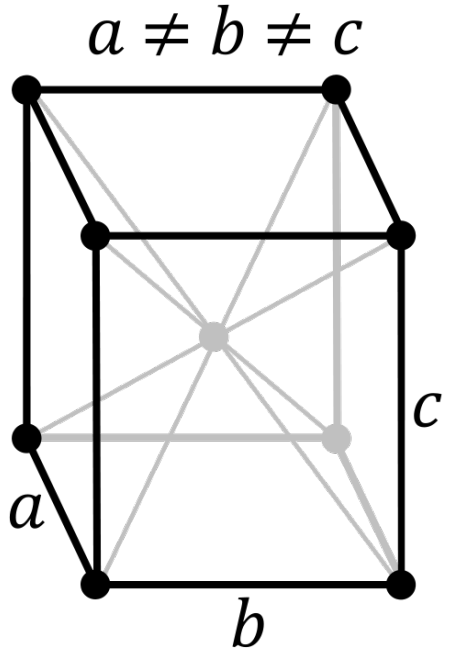

Figure C.6.: Conventional (non-simple) unit cell of the bco lattice

Bibliography

[1] S. Odenbach, Editor, *Ferrofluids, Magnetically Controlable Fluids and Their Applications*, Lect. Notes Phys., Springer, New York (2002).

[2] B. Groh and S. Dietrich, *Crystal structures and freezing of dipolar fluids*, Phys. Rev. E**63**, 021203 (2001).

[3] B. Groh and S. Dietrich, Phys. Rev. E **54**, 1687 (1996).

[4] S. Klapp and F. Forstmann, Europhys. Lett. **38**, 663 (1997).

[5] S. Klapp and F. Forstmann, J. Chem. Phys. **109**, 1062 (1998).

[6] S. Klapp and G. Patey, J. Chem. Phys. **112**, 10 949 (2000).

[7] G. T. Gao and X. C. Zeng, *Freezing transition of a strongly dipolar simple fluid*, Phys. Rev. E **61**, R2188 (2000).

[8] P. P. Ewald, Ann. Phys. (Leipzig) **64**, 253 (1921).

[9] S. W. de Leeuw, J. W. Perram and E. R. Smith, *Simulation of electrostatic systems in periodic boundary conditions. I.Lattice sums and dielectric constants*, Proc. R. Soc. London A, 373: 27-56 (1980).

[10] M. P. Tosi, *Cohesion of ionic solids in the Born model* in F. Seitz and D. Turnbull, editors, Solid State Physics: Advances in Research and Applications, pages 1-120 (Academic Press, New York, 1964).

[11] J. H. Holland, *Adaption in Natural and Artificial Systems* (The University of Michigan Press, Ann Arbor, 1975).

[12] C. Holm and J.-J. Weiss, *The structure of ferrofluids: A status report*, Curr. Opin. Colloid Interface Sci. **10**, issuses 3-4, 133-140 (2005).

[13] J. E. Lennard-Jones, Proc. Roy. Soc., v. A 106, p. 463 (1924).

[14] F. M. Mourits and F. H. A Rummens, *A critical evaluation of Lennard-Jones and Stockmayer potential parameters and of some correlation methods*, Can. J. Chem. **55**, 30073020 (1977).

[15] M. Schoen and S. Klapp, *Reviews in computational chemistry*, volume **24** (Wiley-VCH, 2007).

[16] A. P. Philipse and D. Maas, *Magnetic colloids from magnetotactic bacteria: chain formation and colloidal stability*, Langmuir **18**, 9977-9984 (2002).

[17] A. Bravais, *Mémoire sur les systèmes formés par les points distribués régulirement sur un plan ou dans l'espace*, J. Ecole Polytech. **19** 1128 (1850) (English: *Memoir 1*, Crystallographic Society of America (1949)).

[18] T. M. Nymand and P. Linse, *Ewald summation and reaction field methods for potentials with atomic charges, dipoles, and polarizabilities*, J. Chem. Phys. **112**, 6152 (2000).

[19] A. Smith and N. Ashcroft, Phys. Rev. B **38**, 12 942 (1988).

[20] D. Frenkel and N. Smit, *Understanding molecular simulation* (Academic press, 1996).

[21] J.-M. Caillol, J. Chem. Phys. **101**, 6080 (1994).

[22] M. P. Allen and D. J. Tildesley, *Computer Simulation of Liquids* (Oxford University Press, 1987).

[23] `http://www.cse.scitech.ac.uk/ccg/software/DL_POLY/`

[24] M. Deserno and C. Holm, *How to mesh up Ewald sums. I.A theoretical and numerical comparison of various particle mesh routines*, J. Chem. Phys. **109**, 18 (1998).

[25] M. J. L. Sangster and M. Dixon, Adv. Phys. **25**, 247 (1976).

[26] A. Y. Toukmaji and J. A. Board Jr, *Ewald Summation Techniques in Perspective: A Survey*, Comput. Phys. Commun. **95**, pp. 7392 (1996).

[27] Z. Rycerz and P. Jacobs, Mol. Simulation **8** 197 (1992).

[28] J. W. Eastwood and R. W. Hockney, *Shaping the force law in two-dimensional particle mesh models*, J. Comp. Phys., **16**: 342-359 (1974).

[29] L. Greengard and V. Rokhlin, *A fast algorithm for particle simulations*, J. Comp. Phys., **73**: 325-348 (1987).

[30] J. J. Cerdà, *Tutorial, 8: Long range interactions: Direct sum and Ewald summation*, SimBio group, FIAS, Frankfurt (2007).

[31] T. A. Darden, D. York and L. Pedersen, *Particle mesh Ewald: An N log(N) method for Ewald sums in large systems*, J. Chem. Phys., **98**: 10089-10092 (1993).

[32] C. Darwin, *The Origin of Species by Means of Natural Selection* (John Murray, Albemarle Street, London, 1859).

[33] D. E. Goldberg, *Genetic Algorithms in Search, Optimization and Machine Learning* (Addison-Wesley, MA, 1989).

[34] Z. Michalewicz, *Genetic Algorithms + Data Structures = Evolution Programs* (Springer, New York, 1992).

[35] D. M. Deaven and K. M. Ho, *Molecular Geometry Optimization with a Genetic Algorithm*, Phys. Rev. Lett. **75**, 288 (1995).

[36] D. E. Clark (ed.), *Evolutionary Algorithms in Molecular Design* (Wiley-VCH, Weinheim, 2000).

[37] J. Arifovic, *Genetic algorithm learning and the cobweb model*, J. Econ. Dyn. Contr. **18**, 3 (1994).

[38] T. Riechmann, *Genetic algorithm learning and evolutionary games*, J. Econ. Dyn. Contr. **25**, 1019 (2001).

[39] G. W. Greenwood and A. M. Tyrell, *Introduction to Evolvable Hardware* (Wiley-IEEE Press, 2006).

[40] A. R. Oganov and C. W. Glass, *Crystal structure prediction using* ab initio *evolutionary techniques: Principles and applications*, J. Chem. Phys. **124**, 244704 (2006).

[41] S. M. Woodley and R. Catlow, *Crystal structure prediction from first principles*, Nature Materials **7**, 937-946 (2008).

[42] B. Hartke, *Application of Evolutionary Algorithms to Global Cluster Geometry Optimization*, Struct. Bond. **110**, 33-53 (2004).

[43] D. Gottwald, *Genetic Algorithms in Condensed Matter Theory*, Ph. D. thesis, TU Vienna (2005).

[44] D. Gottwald, G. Kahl and C. N. Likos, *Predicting equilibrium structures in freezing processes*, J. Chem. Phys. **122**, 204503 (2005).

[45] G. J. Pauschenwein, *Phase behavior of colloidal systems*, Ph. D. thesis, TU Vienna (2008).

[46] G. J. Pauschenwein and G. Kahl, *Clusters, columns, and lamellae - minimum energy configurations in core softened potentials*, Soft Matter **4**, 1396 (2008).

[47] G. J. Pauschenwein and G. Kahl, *Zero temperature phase diagram of the square-shoulder system*, J. Chem. Phys. **129**, 174107 (2008).

[48] G. Doppelbauer, *Development of a Phenotype Algorithm for Particle Geometry Optimization*, Master thesis, TU Vienna (2009).

[49] J. Fornleitner, *Ordered Equilibrium Structures of Two-Dimensional Soft Matter Systems*, Ph. D. thesis, TU Vienna (2008).

[50] J. Fornleitner, F. Lo Verso, G. Kahl and C .N. Likos, *Genetic algorithms predict formation of exotic ordered configurations for two-component dipolar monolayers*, Soft Matter **4**, 480 (2008).

[51] J. Fornleitner and G. Kahl, *Lane formation vs. cluster formation in two-dimensional square-shoulder systems - A genetic algorithm approach*, Europhys. Lett. **82**, 18001 (2008).

[52] M. Kahn, *Ordered equilibrium structures of soft particles in layered systems*, Diploma thesis, TU Vienna (2008).

[53] C. W. Glass, A. R. Oganov and N. Hansen, *USPEX - Evolutionary crystal structure prediction*, Comput. Phys. Commun. **175** 713-720 (2006).

[54] Y. Zeiri, *Prediction of the lowest energy structure of clusters using a genetic algorithm*, Phys. Rev. E **51**, 2769-2772 (1995).

[55] J. M Soler, E. Artacho, J. D. Gale, A. Garcia, J. Junquera, P. Ordejon and D. Sanchez-Portal, *The SIESTA method for ab initio order-n materials simulation*, J. Phys.:Condens. Matter **14** 2745-2779 (2002).

[56] G. Kresse and J. Furthmüller, *Efficient iterative schemes for ab initio total-*

energy calculations using a plane wave basis set, Phys. Rev. B **54**, 11169-11186 (1996).

[57] B. Hartke, *Global Cluster Geometry Optimization by a Phenotype Algorithm with Niches: Location of Elusive Minima, and Low-Order Scaling with Cluster Size*, J. Comp. Chem. **20**, 1752-1759 (1999).

[58] R. L. Johnston, *Evolving better nanoparticles: Genetic algorithms for optimising cluster geometries*, Dalton Trans. **2003**, 4193-4207 (2003).

[59] R. H. Byrd, P. Lu and J. Nocedal *A Limited Memory Algorithm for Bound Constrained Optimization*, SIAM J. Sci. Stat. Comp. **16**, 1190-1208 (1995).

[60] C. Zhu, R. H. Byrd and J. Nocedal, *L-BFGS-B: Algorithm 778: L-BFGS-B, FORTRAN routines for large scale bound constrained optimization*, ACM Trans. Math. Software **23**, 550-560 (1997).

[61] `http://www.gromacs.org/Documentation/Terminology`

[62] M. Luescher, *A portable high-quality random number generator for lattice field theory simulations*, Comput. Phys. Commun. **79**, 100 (1994).

[63] F. James, *RANLUX: a Fortran implementation of the high-quality pseudorandom number generator of Lüscher*, Comput. Phys. Commun. **79**, 100 (1994).

[64] A. Miller, *TOMS778*, `http://users.bigpond.net.au/amiller/toms/toms778.zip` (1999).

[65] J.-M. Jin, *FORTRAN routines for computation of Special Functions*, `http://jin.ece.uiuc.edu/routines/routines.html`.

[66] `http://www.mpikg-golm.mpg.de/th/physik/allen_tildesley/allen_tildesley.22`

[67] H. T. Stokes and D. M. Hatch, *FINDSYM*, `http://stokes.byu.edu/findsym.html`

[68] Center for Computational Materials Science, US Navy, `http://cst-www.nrl.navy.mil/lattice/spcgrp/index.html`

[69] *PyMOL Molecular Viewer*, `http://www.pymol.org`.

[70] J. Weis and D. Levesque, Phys. Rev. E **48**, 3728 (1993).

[71] http://www.motionscript.com/mastering-expressions/random-sphere.html

[72] A. Aguado and P. A. Madden, *Ewald summation of electrostatic multipole interactions up to the quadrupolar level*, J. Chem. Phys. **119**, 7471 (2003).

[73] http://en.wikipedia.org/wiki/Bravais_lattice

[74] http://en.wikipedia.org/wiki/Close-packing_of_spheres

Acknowledgements

At first I would like to thank my supervisor Gerhard Kahl for his attention, his advice and his support during this Master Thesis, as well as the whole Soft Matter Theory group at TU Vienna: Daniele Coslovich, Günther Doppelbauer, Jan Kurzidim, Dieter Schwanzer, Lukas Strauss, and also Florian Libisch, for the nice and interesting lunches and the help provided when it was needed. Special thanks to Günther for introducing me to his research subject and for his major help.

Thanks to Martial Mazars, Jean-Jacques Weis and Dominique Levesque of the Laboratoire de physique théorique d'Orsay (CNRS and Université Paris-Sud 11, France) for kindly answering my questions.

My Master at the TU Vienna took place as part of the Top Industrial Manager for Europe (TIME) program and I would like to thank the staff of the BRIF at the Ecole Centrale Paris in France as well as Prof. Peter Schattschneider at the TU Vienna for enabling this rewarding experience of a double diploma in Vienna and for their efficient help.

Thanks also to my family, my boyfriend and my friends both in Vienna and France for supporting and bearing me during this Master.